LEVEL II

12

SC

WATER TUNNEL SIMULATION STUDY OF THE LATER STAGES OF WATER ENTRY OF CONICAL HEAD BODIES: PHASE II - EFFECT OF THE AFTERBODY ON STEADY STATE VENTILATED CAVITIES

D. R. Stinebring and J. W. Holl

Technical Memorandum
File No. TM 79-206
December 3, 1979
Contract No. N00024-79-C-6043

Copy No. 19

The Pennsylvania State University
APPLIED RESEARCH LABORATORY
Post Office Box 30
State College, PA 16801

NAVY DEPARTMENT

NAVAL SEA SYSTEMS COMMAND

Approved for Public Release
Distribution Unlimited

UNCLASSIFIED

SECURITY CLASSIFICATION OF THIS PAGE (When Data Entered)

REPORT DOCUMENTATION PAGE

READ INSTRUCTIONS BEFORE COMPLETING FORM

1. REPORT NUMBER: TM 79-206

2. GOVT ACCESSION NO.: AD-A086980

3. RECIPIENT'S CATALOG NUMBER:

4. TITLE (and Subtitle): (6) Water Tunnel Simulation Study of the Later Stages of Water Entry of Conical Head Bodies, Phase II: Effect of the Afterbody on Steady State Ventilated Cavities

5. TYPE OF REPORT & PERIOD COVERED: Technical Memorandum

6. PERFORMING ORG. REPORT NUMBER:

7. AUTHOR(s): (10) D. R. Stinebring and J. W. Holl

8. CONTRACT OR GRANT NUMBER(s): (15) N00024-79-C-6043

9. PERFORMING ORGANIZATION NAME AND ADDRESS:
Applied Research Laboratory
P.O. Box 30
State College, PA 16801

10. PROGRAM ELEMENT, PROJECT, TASK AREA & WORK UNIT NUMBERS:

11. CONTROLLING OFFICE NAME AND ADDRESS:
Naval Sea Systems Command - Code 63R31
Washington, DC 20362

12. REPORT DATE: December 3, 1979

13. NUMBER OF PAGES: 69

14. MONITORING AGENCY NAME & ADDRESS (if different from Controlling Office): (11) 3 Dec 79

15. SECURITY CLASS. (of this report): UNCLASSIFIED

15a. DECLASSIFICATION/DOWNGRADING SCHEDULE:

16. DISTRIBUTION STATEMENT (of this Report):
Approved for Public Release. Distribution Unlimited. (12) 73
Per NAVSEA - June 27, 1980.

17. DISTRIBUTION STATEMENT (of the abstract entered in Block 20, if different from Report):
(9) Technical memo

18. SUPPLEMENTARY NOTES:
(14) ARL/PSU/TM-79-206

19. KEY WORDS (Continue on reverse side if necessary and identify by block number):
Water Tunnel, cavity running, water entry, conical head, afterbody, cavitation

20. ABSTRACT (Continue on reverse side if necessary and identify by block number):
This report documents the second phase of the water tunnel studies that are intended to simulate the cavity running phase of water entry. The primary purpose of the investigation was to study the effect of afterbody arrangement on steady state ventilated cavities. The models utilized were 1.0 inch diameter conical nosed bodies with a 45° DEG. apex angle. Three models were tested: one having a 1.0 inch diameter afterbody, one having a 0.5 inch diameter afterbody and the third having no afterbody. The cavitation number as a function of cavity length and ventilation air flow coefficient as a function of cavitation

DD FORM 1 JAN 73 1473 EDITION OF 1 NOV 65 IS OBSOLETE

UNCLASSIFIED 394 007

SECURITY CLASSIFICATION OF THIS PAGE (When Data Entered)

20. number were measured for all models. The pressure distribution was found for a wide range of cavity lengths for the model with the 1.0 inch diameter afterbody. Data for the ventilation air flow coefficient and pressure distribution are in good agreement with previous studies of similar models. An interesting result is that the model requiring the lowest ventilation air flowrate for a given cavitation number was the model with no afterbody. For most of the flow states investigated, the model with the 0.5 inch diameter afterbody required the highest flowrate. The transition between the reentrant jet and twin vortex regimes was studies briefly. At transition, the cavity would grow four or five times its original length for a slight increase in ventilation air flowrate. A cavity attrition test was conducted to simulate the decay of a cavity behind a missile. The general agreement between the steady state and instantaneous data was poor. It was felt this was due to the setup utilized in the experiments.

Subject: Water Tunnel Simulation Study of the Later Stages of Water Entry of Conical Head Bodies: Phase II - Effect of the Afterbody on Steady State Ventilated Cavities

References: See Page 22

Abstract: This report documents the second phase of the water tunnel studies that are intended to simulate the cavity running phase of water entry. The primary purpose of the investigation was to study the effect of afterbody arrangement on steady state ventilated cavities. The models utilized were 1.0 inch diameter conical nosed bodies with a 45° apex angle. Three models were tested: one having a 1.0 inch diameter afterbody, one having a 0.5 inch diameter afterbody and the third having no afterbody. The cavitation number as a function of cavity length and ventilation air flow coefficient as a function of cavitation number were measured for all models. The pressure distribution was found for a wide range of cavity lengths for the model with the 1.0 inch diameter afterbody. Data for the ventilation air flow coefficient and pressure distribution are in good agreement with previous studies of similar models. An interesting result is that the model requiring the lowest ventilation air flowrate for a given cavitation number was the model with no afterbody. For most of the flow states investigated, the model with the 0.5 inch diameter afterbody required the highest flowrate. The transition between the reentrant jet and twin vortex regimes was studied briefly. At transition, the cavity would grow four or five times its original length for a slight increase in ventilation air flowrate. A cavity attrition test was conducted to simulate the decay of a cavity behind a missile. The general agreement between the steady state and instantaneous data was poor. It was felt this was due to the setup utilized in the experiments.

Acknowledgements

The research presented in this report was conducted in the Fluids Engineering Department (FED) of the Applied Research Laboratory at The Pennsylvania State University. The FED is located in the Garfield Thomas Water Tunnel Building. The research was sponsored by the Naval Sea Systems Command, Code 63R31.

The assistance of R. W. Woods is gratefully acknowledged in setting up the data acquisition system. The advice and counsel of M. L. Billet during the test program is also gratefully acknowledged.

Table of Contents

List of Tables

List of Figures

List of Figures (cont)

Nomenclature

A_0	Cross-sectional area of the tunnel stagnation section
A(x)	Cross-sectional area at x
C_{P_i}	Pressure coefficient at pressure tap i
C_Q	Ventilation air flow coefficient
D	Model Diameter
Fr	Froude number $V_\infty/\sqrt{g\ D}$
g	Gravitational constant (32.2 ft/sec^2)
k^*	Critical cavitation number for the transition from the twin vortex to reentrant jet regime
L	Cavity length
P_c	Cavity pressure
P_{G-S}	Partial pressure of dissolved gas at saturation
P_i	Pressure at tap i
P_0	Total pressure
P_∞	Free-stream static pressure
$\dot{Q}$	Volume flowrate of ventilation air
Re	Reynolds number $V_\infty D/\nu$
S	Distance along the model
s	Surface tension
t	Time
V_∞	Free-stream velocity
We	Weber number $V_\infty\sqrt{\frac{D}{s/\rho}}$

x_0 Position of the beginning of the tunnel stagnation section

x_∞ Position of the beginning of the tunnel test section

α Air content

β Henry's Law constant

ν Kinematic viscosity

ρ Mass density of the working fluid

σ Cavitation number

σ_p Instantaneous cavitation number based on $P_0(t) - P_\infty(t)$

σ_t Instantaneous cavitation number based on the instantaneous velocity in the test section

σ^* Critical cavitation number for the transition from the reentrant jet to twin vortex regime

I. INTRODUCTION

When a missile passes from a gaseous to a liquid environment many factors influence the resulting trajectory. As indicated on page 3, section 1 of May [1]* the body shape, entry velocity and attitude affect the eventual path of the projectile. Water entry phenomena are usually investigated in a hydroballistics tank, where the model is fired into a stationary tank of water at the desired velocity and entry angle. Extensive instrumentation is required for recording the rapid sequence of events in the entry cycle which generally has the following phases:

1. Shockwave Phase
2. Flow-Forming Phase
3. Open-Cavity Phase
4. Closed-Cavity Phase
5. Collapsing-Cavity Phase
6. Fully Wetted Phase

An explanation of these phases can be found in Reference 1.

A study of the growth and attrition of the cavity formed over a body is of great importance. In many instances the cavity will extend far behind the missile. The control surfaces then may have only limited contact with the water and the missile trajectory can be erratic. The point at which the cavity shortens to an extent that the control surfaces are again effective is of vital interest.

The closed-cavity and collapsing-cavity phases are of interest in this investigation and together constitute the cavity running phase of water entry. When this phase is reached, the missile and trailing cavity are isolated from the free surface. If the cavity running phase could be simulated in a water tunnel environment, the problem would be greatly simplified. It is for this reason that this investigation has been undertaken.

Previous studies of this subject have been conducted at the Garfield Thomas Water Tunnel by Kim and Holl [2]. This first study was concerned with cavity geometry, ventilation air flow rate, pressure distribution, and cavity attrition for a series of conical-nosed bodies with ventilated cavities. The present investigation is an extension of the previous work. Of main consideration is the influence of the afterbody arrangement on the entrainment rate, cavitation number, and attrition rate. In addition it was desirable to extend the pressure distribution data by Kim and Holl [2] to longer cavity lengths.

The investigation was conducted in four main parts. In the first part the cavitation number was measured as a function of cavity length. The second part involved the measurement of the ventilation air flow coefficient as a function of cavitation number. In the third part, the pressure distribution

* Numbers in brackets refer to documents in list of references.

was measured on the body with the 1.0 inch afterbody. Lastly, a study of the cavity decay process was conducted using the model with no afterbody. For the cavity attrition test the tunnel drive and ventilation air were turned off simultaneously to simulate the later stages of a cavity running missile. The decay of the cavity was recorded photographically while instantaneous measurement of the cavity and free-stream pressures were measured. A comparison between the cavity attrition and steady state data could then be made.

II. DESCRIPTION OF THE EXPERIMENTAL INVESTIGATION

2.1 Test Models

The test facility used throughout this investigation was the 12-inch water tunnel located in the Garfield Thomas Water Tunnel Building of the Applied Research Laboratory at The Pennsylvania State University. This facility is capable of maximum velocities of approximately 70 ft/sec and is equipped with extensive degassing equipment for varying the total air content. There were three models employed during this investigation:

Model I - 45° apex angle, 1.0 inch diameter conical head joined to a 0.5 inch diameter afterbody

Model II - 45° apex angle, 1.0 inch diameter conical head joined to a 1.0 inch diameter afterbody

Model III - 45° apex angle, 1.0 inch diameter conical head without an afterbody and supported by three struts

A photograph of these models is shown in Figure 1. Each model was fabricated with six holes around the periphery where the conical nose joins the afterbody, for the introduction of ventilation air. A pressure tap was located on all models for measuring the cavity pressure. The model with the 1.0 inch afterbody also contained a total of nine pressure taps along the conical nose and afterbody for measuring the pressure distribution.

The tests were conducted at velocities of 30, 45, and 50 ft/sec with the flow velocity set by knowing calibrations with a pressure transducer from previous tests. The experimental setup for the steady state measurements is illustrated in Figure 2.

2.2 Cavitation Number Versus Cavity Length

The first test was to determine the relationship between the cavitation number (σ) and the cavity length. The ventilation air was turned on after attaining the test velocity and the cavity length was then set by observing lines which were on the afterbody every 0.5 inch. The cavity length was judged in a somewhat different manner for the model with no afterbody. A graduated rule was taped to the windows on either side of the tunnel. By sighting across the test section and lining up the correct scales, the cavity length could be set accurately. The pressures, P_0-P_∞, P_∞ and P_c where P_0 is the total pressure, P_∞ is the free-stream static pressure and P_c is the cavity pressure, were then measured for computing the cavitation number.

2.3 Ventilation Air Flow Coefficient

One of the main objectives of this investigation involved recording the effect of the afterbody arrangement on the entrainment rate. Careful consideration was given to the experimental procedure so that gaseous diffusion across the cavity wall was minimized. The test sequence was as follows:

1) Initially the tunnel was run to insure that the air content was uniform throughout the tunnel with any large amounts of free gas being bled off at the domes.

2) An air content reading, taken with a Van Slyke apparatus, measured the total gas content. During this time the tunnel pressure was kept high enough so that air would not come out of solution.

3) The test parameters (P_0-P_∞, P_c, P_∞, and σ) were then selected pending the results of the air content reading. In general, a high air content necessitated testing at the shorter cavity lengths and visa versa. This was required to keep the pressure in the flowmeter within safety limits.

4) The cavity pressure for minimum diffusion was then calculated according to Henry's Law i.e. the cavity pressure (P_c) was set equal to the partial pressure of air at saturation i.e. $\alpha\ \beta$ where α is the air content in ppm and β is Henry's law constant.

5) The test section static pressure (P_∞) was calculated for the given cavity pressure, flow velocity and cavitation number i.e. $P_\infty = 1/2\rho V_\infty^2 \sigma + P_c$ where ρ is the density of the water.

6) After setting the tunnel conditions the air supply was turned on until the correct cavity length was achieved.

7) The flowmeter reading, flowmeter pressure, P_0-P_∞, P_∞, and P_c were measured a number of times during the test. (If there was relatively little air injected into the system during the test such as for shorter cavity lengths, another test could quickly be run before the air content had changed appreciably.)

8) The tunnel pressure was decreased at the conclusion of the run and much of the free air bled off through the domes which required from 10 to 30 minutes.

9) Pressurizing the tunnel then pushed the remaining free air into solution.

10) The test cycle was then repeated.

2.4 Pressure Distribution

As previously mentioned, the model with the 1.0 inch diameter afterbody was equipped with nine pressure taps for measuring the pressure distribution over the body. The apparatus for this test is similar to that shown in Figure 2, with the exception of a multichannel scanivalve replacing the manual pressure switches and the output of the pressure transducer recorded on a teletype.

The tunnel was brought up to the test velocity and the air flowrate increased to adjust the cavity length to the desired value. A number of readings at each condition were taken. Care was taken to insure that the cavity length did not vary appreciably during the time of the data collection.

2.5 Cavity Attrition

The cavity attrition tests were conducted at velocities of 30 and 50 ft/sec for a range of cavity lengths with the procedure similar to that of Kim and Holl [2]. The test setup is illustrated in Figure 3 and test procedure is as follows:

1. All pressure transducers were first bled and zeroed.
2. The framing rate and aperture setting of the movie camera used for recording the collapse cycle were set.
3. The tunnel velocity and pressure were adjusted to the desired test conditions.
4. A stopwatch in the field of view of the movie camera was started. This allowed an accurate calibration of the movie camera framing rate.
5. Photographic lights illuminating the tunnel test section were turned on.
6. The ventilation air was adjusted for the correct cavity length.
7. The movie camera and oscillograph were started.
8. To initiate the test sequence the ventilation air supply and tunnel drive system were shut down simultaneously. A strobe light connected to the tunnel drive switch, also fired at this time.
9. After the completion of the cavity decay, the movie camera was switched off and zero valves for the oscillograph traces were found after each test.

The data for the cavity attrition tests were in the form of a movie sequence and an oscillograph trace. The point at which the tunnel drive was shut down was marked on the movie film by a darkened frame due to the strobe flash. A photoelectric cell simultaneously created a pulse on the oscillograph trace at the instant of the strobe flash. Also P_0, P_∞ and P_c were recorded on the oscillograph for calculating the cavitation index as a function of time. By comparing the movie sequence and the oscillograph traces the instantaneous cavitation number as a function of instantaneous cavity length could be found.

III. TEST RESULTS AND DISCUSSION

3.1 Cavitation Number Versus Cavity Length

The cavitation number is defined as

$$\sigma = \frac{P_\infty - P_c}{1/2\rho V_\infty^2} \tag{1}$$

where P_∞ is the free-stream static pressure, P_c is the cavity pressure, ρ is the mass density of the working fluid and V_∞ is the free-stream velocity. Also, the cavity length (L) was expressed in the dimensionless form

$$L/D = \frac{\text{Cavity Length}}{\text{Model Diameter}} \quad . \tag{2}$$

Data for the three models at velocities of 30, 45, and 50 fps are tabulated in Table 1 and presented in Figures 4-6 with the empirical equation which correlates the data shown in each figure. Figure 7 presents a comparison of the data for all three models. In this figure, the average cavitation number at the three velocities for a given cavity length was plotted for each model. The data for all three models are closely approximated by a single curve. A comparison of the data for this investigation and that of Kim and Holl [2] is presented in Figure 8. At the shorter cavity lengths, the data of Kim and Holl are slightly higher than the corresponding data obtained in this investigation. After examination of the models for both investigations, it was observed that the junction point between the cone and afterbody was slightly rounded for the present study. In contrast, the junction point on the model utilized by Kim and Holl was a sharp angle. This rounded edge could have a significant effect upon the flow field which would tend to decrease the cavitation number for a given L/D.

3.2 Ventilation Air Flow Coefficient

The ventilation air flow coefficient is defined as

$$C_Q = \frac{\dot{Q}}{V_\infty D^2} \tag{3}$$

where $\dot{Q}$ is the volume flowrate of air needed to sustain a given cavity, V_∞ is the upstream velocity, and D is the model diameter. The effect of diffusion across the cavity wall was minimized by maintaining the average cavity pressure equal to the partial pressure of the gas at saturation. The partial pressure of the gas at saturation is obtained by Henry's Law given by

$$P_{G-S} = \alpha\beta \tag{4}$$

where α is the dissolved air content and β is the Henry's Law constant at the bulk temperature of the water. For minimum diffusion then $P_c = P_{G-S}$ so that

$$\sigma = \frac{P_\infty - P_{G-S}}{1/2\rho V_\infty^2} \tag{5}$$

and

$$P_\infty = 1/2\rho V_\infty^2 \sigma + P_{G-S} \tag{6}$$

The air content was measured with a Van Slyke apparatus. (The total gas content as measured by the Van Slyke apparatus is the dissolved gas content plus the free gas content. Since the free gas content is a small part of the total gas content, the value obtained by the Van Slyke apparatus closely approximates the dissolved gas content.) As stated previously, σ is a function of cavity length, so for a given set of test parameters and a measured air content, the free-stream pressure can be set for minimum diffusion across the cavity wall.

In addition to limiting the effects of gaseous diffusion, vaporous cavitation had to be eliminated. This was done by operating the tunnel at sufficiently high free-stream static pressures. With gaseous diffusion and vaporization minimized, an accurate measurement of the rate of air flow out of the cavity could be made.

The flow coefficient as a function of cavitation number is presented for the three models in Figures 9 to 11 and the data are tabulated in Table 2. The results show the same qualitative trend as observed by Kim and Holl [2] and Billet and Weir [2], namely an increase in C_Q with both velocity and cavity length.

In Figure 12, an interesting comparison is made between the ventilation air flow coefficients as a function of cavitation number for all three models. These results are presented for a velocity of 45 ft/sec. The model requiring the lowest flowrate for a given cavitation number is the one with no afterbody. The model with the 0.5 inch diameter afterbody required the largest flowrate except at the highest values of σ. The data for the model with the 1.0 inch diameter afterbody was between other two.

It would seem that the model with no afterbody should require the largest flowrate because of the apparent greater volume of gas inside the cavity but this was not the case. The reentrant jet behavior could possibly account for this effect. It is indicated on page 32 of Section 3 of Reference [1] that the mixing created by the reentrant jet is the main entrainment mechanism. Due to gravity effects, the reentrant jet should move along the bottom of the cavity for the model with no afterbody. An afterbody could have a guiding effect upon the reentrant jet causing more mixing in the upper section of the cavity. Observations of the cavity support this contention. The fact still remains that the model with the 0.5 inch diameter afterbody required a greater flowrate than the model with the 1.0 inch diameter afterbody. However, considering the possible data spread it may be that the data for the bodies with 0.5 inch and 1.0 inch afterbodies are fairly close to each other.

Also in Figure 12 some of the data of Kim and Holl [2] for a model with a 1.0 inch afterbody are plotted. For this test condition there is good agreement between the Kim-Holl data and the data for Model II.

3.3 Pressure Distribution

The pressure was expressed as a dimensionless quantity in the form

$$C_{P_i} = \frac{P_i - P_\infty}{1/2\rho V_\infty^2} \tag{7}$$

where P_i is the pressure at tap i(i=1 to 9). The pressure distribution results are shown in Figures 13-15 and the data are tabulated in Table 3. It is noted in Figures 13-15 that $\sigma \simeq |C_p|$ for the pressure taps in the cavity i.e. taps 8 and 9. These data were obtained to extend the results of Kim and Holl [2] to longer cavity lengths. The results for one condition, compared to data taken by Kim and Holl and Rouse and McNown [4], are shown in Figure 16. There is good agreement for all points except at pressure tap 7 where Kim and Holl recorded a somewhat lower C_p. This is most likely due to the fact that the slope of the pressure distribution in this area is very steep. A small change in the location of the tap would cause a large variation in the measured pressure.

It is apparent from Figure 16 that the position of the pressure taps for this investigation do not coincide with those for the other investigations. The exact pressure tap locations for the two models are given in Table IV.

3.4 Observations of the Transition Between the Reentrant Jet and Twin Vortex Flow Regimes

A very interesting observation was made during the study of the model with no afterbody. It was noticed that when the cavity reached a certain length for given flow conditions it suddenly grew to four or five times its original length. This effect was more pronounced as the velocity was decreased. At 30 ft/sec the cavity length could only be increased to $L/D \approx 5.5$ before becoming unstable. A slight increase in the ventilation air flowrate at this point and the cavity grew to $L/D \approx 25$ (the exact cavity length could not be ascertained since the trailing edge was not visible downstream of the test section window). The flowrate could then be decreased substantially without affecting the cavity length a significant amount. A critical value was reached, upon decreasing the flowrate, where the cavity suddenly shortened to a value of $L/D \approx 2.5$. At other velocities, the critical cavity length and flowrates were different and are summarized in Table V.

The instability in the cavity length may be attributed to the transition between the reentrant jet and twin vortex flow regimes. This effect has been observed in the past and is easily explained. When the cavity is short, there is a reentrant jet formed at the downstream end of the cavity. The reentrant jet moves forward striking the sides of the cavity and in some cases has enough momentum to reach the nose of the model itself. As the cavity becomes longer gravitational effects become significant distorting the streamlines from the axisymmetric case. Because of gravitational effects and an assumed uniform pressure within the cavity, the velocity must be greater on the top of the cavity than on the bottom, resulting in a net circulation.

The reason for the rapid increase in length at transition could be due to the following. The reentrant jet moving through the cavity creates a violent mixing action and thus a very high gas entrainment. As gravitational effects become significant, the cavity becomes more stable, with the reentrant jet eliminated. At this cavity length the ventilation needed to sustain a cavity with a reentrant jet is far greater than that required in the twin vortex regime. The cavity then grows rapidly to a point where equilibrium is reached.

A photograph of the cavity in the reentrant jet regime is shown in Figure 17. The opaque appearance of the cavity is due to the violent mixing caused by the reentrant jet striking the cavity wall. As transition to the twin vortex regime takes place, the cavity becomes clearer at the upstream end with some mixing due the reentrant jet still occurring as shown by the pohtograph in Figure 18. The photograph in Figure 19 shows the cavity in the twin vortex regime at a velocity of 30 fps. For this test condition the cavity extends downstream of the test section window. At approximately 15 fps the cavity in the twin vortex regime is much shorter as shown in Figure 20. The cavity walls are clear and smooth for the twin vortex regime and thus appears very unlike the reentrant jet regime.

Detail of the aft section of the cavity is shown in Figure 21. From this viewing angle only one of the vortices was visible, with the other vortex directly behind the one nearest the camera. Both vortices were

observed when viewed from above the water tunnel test section. Photographs could not be taken at this angle due to the poor optical condition of the upper window in the test section

The gravitational effect upon the transition between flow regimes is shown in Figure 22 where the inverse of the Froude Number is plotted against the critical cavitation index. The critical cavitation index (σ^*) is defined as the lowest possible σ which can be attained before transition to the twin vortex regime occurs. The data indicates

$$Fr\ \sigma^* \approx 3. \tag{8}$$

A similar plot was presented by Swanson and O'Neill [5] for flow over sharp-edged disks. For their investigation the data show that

$$Fr\ k^* \approx 1, \tag{9}$$

where k^* is a critical cavitation number for transition from the twin vortex to the reentrant jet regimes. One possible reason for the lack of agreement between equations 8 and 9 could be the difference in the flow geometries. Another reason for the discrepancy may be due to the difference in the method of determining the critical cavitation indices k^* and σ^*. As just stated, σ^* is the point at which transition from the reentrant jet to the twin vortex regime occurs while increasing the ventilation air flow rate. Swanson and O'Neill evaluated k^* in a somewhat different manner; they measured the critical cavitation number for transition from the twin vortex regime to the reentrant jet regime by decreasing the ventilation air flow rate until the cavity abrubtly shortened.

The difference between σ^* and k^* can be explained by referring to Figure 23, where the ventilation air flow coefficient is plotted as a function of cavitation number. For this investigation the ventilation air flow was increased to point 1 on the graph where transition to the twin vortex regime occurs. This is the value of σ^*. The cavity then grows, without an increase in the ventilation air flowrate, to the conditions indicated by point 2. The flowrate can then be decreased to where transition to the reentrant jet regime occurs, point 3. This would be k^* as defined by Swanson and O'Neill. The cavity then shortens to the flow conditions indicated by point 4.

The method for determining σ^* will give values for σ^* greater than k^*. This would account for some of the difference between the product of the cavitation number and reciprocal of the Froude number as measured by Swanson and O'Neill and by this investigation. Tunnel blockage effects could also influence the results.

The transition region was also observed for the models with afterbodies although the effect was not as pronounced. The full growth of the cavity, when in the twin vortex regime, could not be realized because of interference at the downstream end of the cavity caused by the support strut. Due to the time element involved, further study of the transition between the reentrant jet and twin vortex regime could not be undertaken in this investigation.

3.5 Cavity Attrition

Much of the theoretical analysis for the cavity attrition test is presented in Reference 2. It can be shown that in a decelerating flow

$$1/2\rho V_\infty^2(t) > P_0(t)-P_\infty(t) \quad . \tag{10}$$

If the decelerating effect is great, the difference between the two can be significant. We can, therefore, express the cavitation number in two forms: namely

$$\sigma_p = \frac{P_\infty(t) - P_c(t)}{P_0(t) - P_\infty(t)} \tag{11}$$

or

$$\sigma_t = \frac{P_\infty(t) - P_c(t)}{1/2\rho V_\infty^2(t)} \tag{12}$$

where $P_\infty(t)$, $P_0(t)$, and $P_c(t)$ are the instantaneous pressures in the test section, stagnation section, and cavity pressure, respectively, and $V_\infty(t)$ is the instantaneous velocity in the test section. For steady flow then $\sigma_p = \sigma_t$. From the unsteady Bernoulli equation along the center streamline of the 12 inch water tunnel (contraction ratio of 3:1), it was shown that

$$C_0\dot{V}_0(t) + 40V_0^2(t) + \frac{P_\infty(t) - P_0(t)}{\rho} = 0 \tag{13}$$

where

$$C_0 = A_0 \int_{x_0}^{x_\infty} \frac{dx}{A(x)} . \tag{14}$$

The constant, C_0, was calculated by Kim and Holl [2] to be 24.15 by numerical integration between the pressure tap locations for P_0 and P_∞. Therefore

$$24.15\dot{V}_0(t) + 40V_0^2(t) + \frac{P_\infty(t) - P_0(t)}{\rho} = 0 \tag{15}$$

This equation can be numerically integrated for $V_0(t)$ using the values of $P_0(t) - P_\infty(t)$ from the oscillograph tracings.

Kim and Holl found the deceleration of the tunnel to be on the order of 3 ft/sec^2. This corresponds to less than a three percent difference between σ_p and σ_t. The tunnel velocity history after shutdown for this investigation is shown in Figure 24. The deceleration in the tunnel is approximately 1 ft/sec^2 during the first 0.75 seconds and increases to approximately 6 ft/sec^2 after one second. The attrition time for all cavities in the reentrant jet regime is less than 0.75 seconds, resulting in less than a two percent difference between σ_p and σ_t. For this reason σ_p is plotted in Figures 25 to 27 to simplify calculations. In addition, the velocities in Figure 24 are computed based on the steady state Bernoulli equation. For the time period of interest, namely the first 0.75 seconds, the error would be about one percent.

The results of the cavity attrition tests using Model III are presented in Table VI and in Figures 24 to 27. The agreement between the steady state data and instantaneous measurements is poor with σ_p generally lower than the steady state conditions. It is felt that this discrepancy is primarily due to the test procedure employed in the investigation. The tunnel drive shutdown and strobe flash were connected by a single switch while the ventilation air was shut off with another. Due to the test setup involved, it was necessary to have one person for each switch and to synchronize the tripping of the switches with a countdown. A major source of error could be the difference in reaction times between the two people used during the shutdown procedure. Also, there is a small but finite time for the ventilation air switch to close fully. The dissipation of the total cavity from L/D=6 was usually less than 0.5 seconds, thus a small error due to reaction time and the other factors could have a significant effect on the results.

The data presented in Figure 27 shows the results of runs initially in the twin vortex regime at the time the air supply and tunnel drive were shut down. It is interesting to note that these data are significantly below the data for runs initially in the reentrant jet regime. The exact reason for this is not known, but it may be related to the transition between the twin vortex and reentrant jet regimes described in an earlier section. Also, referring to Table VI, the times for the cavities to dissipate when in the twin vortex regime is far greater than when in the reentrant jet regime.

In Figure 26, data are also given for the case where the ventilation air supply was turned off but the tunnel continued to run. The results are similar to those obtained when both the tunnel drive and air supply were shut off. This indicates that the decelerations encountered during the tunnel shutdown have little influence on the results. Further tests are needed with a better data acquisition system to confirm this result.

IV. CONCLUSIONS AND RECOMMENDATIONS

(1) There was a slight discrepancy between this investigation and that of Kim and Holl [2] for the σ versus L/D data. It is felt that this is due to a difference in contours between the two models.

(2) The σ versus L/D data fall on approximately the same curve for the three models.

(3) The ventilation air flow coefficient as a function of cavitation number follows the same qualitative trends as Kim and Holl [2] and Billet and Weir [3]. The actual flowrates for the cases observed were in good agreement with those of Kim and Holl [2].

(4) An interesting observation concerning the flowrate data is that the model requiring the least amount of ventilation air at a given cavitation number, was the model with no afterbody, whereas the model requiring the greatest amount of air was the one with the 0.5 inch diameter afterbody.

(5) The pressure distribution along the model with the 1.0 inch diameter afterbody showed good agreement with the results of Kim and Holl [2], and Rouse and McNown [4]. In addition, data were obtained for a wide range of cavity lengths at three velocities to extend the data of Kim and Holl [2].

(6) The transition from the reentrant jet to the twin vortex regime was observed, and the effect was most pronounced for the model with no afterbody. Transition was quite sudden with the cavity growing four or five times its original length for a small increase in ventilation air flow rate.

(7) The agreement between the instantaneous cavitation number as a function of cavity length and the steady state data was quite poor. It was felt that the discrepancy was due to the experimental method employed.

(8) Future studies should be conducted along the following lines:

1. Extensive study should be conducted of the transition between the reentrant jet and twin vortex flow regimes. This phenomenon may be of interest in the study of missile trajectories where buoyancy effects are significant.

2. Future models should all be supported by struts attached to the nose, as was done with the model with no afterbody. Models with afterbodies could also be constructed in this manner. This would then eliminate obstruction at the downstream end of the cavity and could more closely approximate prototype conditions.

3. Further work should be conducted on cavity attrition. A fully automated shutdown and data acquisition system could be developed. It was found that the deceleration of the tunnel was initially 1 ft/sec^2 after the tunnel was shut down and increased to 6 ft/sec^2 shortly thereafter. Conducting attrition tests in the period where the deceleration is maximum would more closely approximate water entry. Also a method for increasing the tunnel deceleration in the tunnel should be investigated.

V. REFERENCES

[1] May, A., "Water Entry and Cavity-Running Behavior of Missiles," Naval Sea Systems Command Hydroballistics Advisory Committee Technical Report 75-2, 1975.

[2] Kim, J. H. and Holl, J. W., "Water Tunnel Simulation Study of the Later Stages of Water Entry of Conical Head Bodies," Applied Research Laboratory, Technical Memorandum 75-177, June 18, 1975.

[3] Billet, M. L. and Weir, D. S., "The Effect of Gas Diffusion and Vaporization on the Entrainment Coefficient for a Ventilated Cavity," Applied Research Laboratory Technical Memorandum 74-15, January 24, 1974. (See also Billet, M. L. and Weir, D. S., "The Effect of Gas Diffusion on the Flow Coefficient for a Developed Cavity," Trans. ASME, J. of Fluids Engineering, December 1975, pp. 501-506.)

[4] Rouse, H. and McNown, J. S., "Cavitation and Pressure Distribution, Head Forms at Zero Angle of Yaw," Studies in Engineering, Bulletin 32, State University of Iowa, 1948.

[5] Swanson, W. M. and O'Neill, J. P., "The Stability of an Air-Maintained Cavity Behind a Stationary Object in Flowing Water," CIT Hydrodynamics Report M-24.3, 1951.

[6] Billet, M. L., Holl, J. W., and Weir, D. S., "Correlations by the Entrainment Theory of Thermodynamic Effects for Developed Cavitation in Venturis and Comparisons with Ogive Data," ARL TM 75-291, Dec. 11, 1975 (or NASA CR-135018).

[7] Holl, J. W., Billet, M. L. and Weir, D. S., "Tabulation and Summary of Thermodynamic Effects Data for Developed Cavitation on Ogive-Nosed Bodies," ARL TM 78-18, January 30, 1978 (or NASA CR-135394).

December 3, 1979
DRS:JWH:cac

TABLE I

Tabulation of σ Versus L/D Data

Model I: 1.0 inch Diameter 45° Cone 0.5 inch Afterbody

L/D	σ(Cavitation Number)			Average σ
	30 fps	45 fps	50 fps	(30, 45, 50 fps)
1.5	0.343	0.353	0.357	0.351
2.0	0.318	0.318	0.320	0.319
2.5	0.259	0.276	0.265	0.267
3.0	0.258	0.231	0.232	0.240
3.5	0.206	0.193	0.217	0.205
4.0	0.196	0.189	0.194	0.193
5.0	0.149	0.147	0.165	0.154
6.0	0.093 *	0.131	0.129	0.130
7.0	0.122	0.118	0.109	0.116
8.0	0.115	0.101	0.093	0.103

* Not counted in average σ tabulation

TABLE I - CONTINUED

Model II: 1.0 inch Diameter 45° Cone 1.0 inch Afterbody

L/D	σ(Cavitation Number)			Average σ (30, 45, 50 fps)
	V_∞ = 30 fps	V_∞ = 45 fps	V_∞ = 50 fps	
0.5	0.435	0.446	0.401	0.427
1.0	0.343	0.368	0.372	0.361
1.5	0.305	0.302	0.305	0.304
2.0	0.263	0.256	0.262	0.260
2.5	0.221	0.222	0.230	0.224
3.0	0.203	0.199	0.200	0.201
4.0	0.173	0.166	0.161	0.167
5.0	0.131	0.137	0.141	0.136
6.0	———	0.123	0.129	0.126
7.0	———	———	0.112	0.112
9.0-10.0	0.084	0.098	0.097	0.093

TABLE I - CONTINUED

Model III: 1.0 inch Diameter 45° Cone No Afterbody

L/D	σ(Cavitation Number)			Average σ (30, 45, 50 fps)
	V_∞= 30 fps	V_∞= 45 fps	V_∞= 50 fps	
2.0	0.288	0.295	0.297	0.293
3.0	0.204	0.209	0.200	0.204
4.0	0.166	0.166	0.164	0.165
5.0	0.146	0.136	0.135	0.139
6.0	———	0.119	0.122	0.121
7.0	———	0.115	0.118	0.117
8.0	———	———	0.100	0.100
~25	0.103	0.085	0.086	0.091

TABLE II

Tabulation of C_Q Data

Model I: 1.0 inch Diameter 45° Cone 0.5 inch Afterbody

30 fps

σ	Q cfs	C_Q	P_∞ psia	P_c psia	Average* σ	Average* C_Q
0.336	0.0019	0.0090	24.06	22.03		
0.318	0.0056	0.0267	14.07	12.15		
0.307	0.0048	0.0229	23.56	21.70		
0.251	0.0096	0.0461	16.12	14.60		
0.206	0.0115	0.0552	14.81	13.56	0.204	0.0610
0.201	0.0143	0.0687	14.56	13.35		
0.186	0.0155	0.0744	15.33	14.20		
0.161	0.0158	0.0751	15.94	14.97	0.161	0.0760
0.161	0.0160	0.0766	15.32	14.35		
0.123	0.0181	0.0870	17.63	16.89	0.122	0.0833
0.122	0.0170	0.0815	17.87	17.13		
0.080	0.0195	0.0936	15.30	14.81		

* An average σ and C_Q is presented where σ is close for two tests. These average values account for the number of test points taken for each test.

TABLE II - CONTINUED

Model I: 1.0 inch Diameter 45° Cone 0.5 inch Afterbody

V_∞ = 45 fps

σ	Q (cfs)	C_Q	P_∞ (psia)	P_C (psia)	Average* σ	Average* C_Q
0.356	0.0012	0.0039	21.49	16.65	0.355	0.0046
0.354	0.0015	0.0049	28.50	23.68		
0.323	0.0076	0.0244	23.26	18.86		
0.304	0.0066	0.0210	16.50	12.36		
0.267	0.0144	0.0461	21.53	17.90		
0.241	0.0180	0.0577	22.13	18.98		
0.229	0.0197	0.0631	21.06	17.95	0.228	0.0606
0.226	0.0179	0.0572	16.23	13.15		
0.195	0.0208	0.0665	18.17	15.51		
0.168	0.0239	0.0765	18.74	16.45		
0.135	0.0283	0.0906	17.28	15.44		
0.122	0.0292	0.0935	15.90	14.24	0.121	0.0979
0.120	0.0317	0.1015	16.71	15.08		
0.109	0.0328	0.1049	17.66	16.18		
0.0899	0.0373	0.1192	16.65	15.42		

* These average values account for the total number of data points for each run.

TABLE II - CONTINUED

Model I: 1.0 inch Diameter 45° Cone 0.5 inch Afterbody

V_∞ = 50 fps

σ	Q (cfs)	C_Q	P_∞ (psia)	P_C (psia)	Average* σ	Average* C_Q
0.350	0.0017	0.0048	20.87	14.98		
0.309	0.0082	0.0237	20.40	15.20		
0.280	0.0135	0.0390	20.92	16.21	0.275	0.0424
0.271	0.0159	0.0458	24.26	19.70		
0.239	0.0190	0.0547	22.57	18.55		
0.221	0.0230	0.0662	23.52	19.80		
0.185	0.0257	0.0741	19.26	16.15		
0.140	0.0307	0.0883	20.26	17.90		
0.123	0.0310	0.0892	16.42	14.35		
0.117	0.0368	0.1061	16.82	14.85		
0.0839	0.0421	0.1213	15.96	14.55		

* These average values account for the total number at data points for each run.

TABLE II - CONTINUED

Model II: 1.0 inch Diameter 45° Cone 1.0 inch Afterbody

V_∞ = 30 fps

σ	Q (cfs)	C_Q	P_∞ (psia)	P_C (psia)
0.390	0.0013	0.0063	19.98	17.62
0.384	0.0030	0.0143	19.51	17.19
0.306	0.0052	0.0248	19.48	17.63
0.251	0.0070	0.0336	20.92	19.40
0.212	0.0090	0.0432	19.90	18.61
0.182	0.0098	0.0469	19.79	18.69
0.144	0.0131	0.0630	22.33	21.46
0.130	0.0142	0.0681	19.15	18.36
0.090	0.0142	0.0681	18.48	17.94

TABLE II - CONTINUED

Model II: 1.0 inch Diameter 45° Cone 1.0 inch Afterbody

V_∞ = 45 fps

σ	Q (cfs)	C_Q	P_∞ (psia)	P_C (psia)
0.412	0.0023	0.0072	28.69	23.08
0.386	0.0058	0.0185	23.67	18.42
0.310	0.0881	0.0282	22.13	17.91
0.271	0.0130	0.0417	26.48	22.79
0.230	0.0158	0.0507	24.24	21.10
0.209	0.0175	0.0560	22.32	19.47
0.178	0.0217	0.0694	21.41	18.99
0.142	0.0239	0.0764	16.59	14.66
0.122	0.0254	0.0813	15.41	13.75
0.085	0.0268	0.0857	15.86	14.70

TABLE II - CONTINUED

Model II: 1.0 inch Diameter 45° Cone 1.0 inch Afterbody

V_∞= 50 fps

σ	Q (cfs)	C_Q	P_∞ (psia)	P_C (psia)
0.395	0.0025	0.0071	27.05	20.42
0.390	0.0064	0.0185	23.84	17.31
0.300	0.0105	0.0301	23.46	18.43
0.258	0.0145	0.0417	26.02	21.70
0.228	0.0175	0.0504	26.07	22.25
0.208	0.0202	0.0581	23.93	20.44
0.165	0.0242	0.0697	17.89	15.13
0.142	0.0290	0.0836	15.47	13.09
0.141	0.0266	0.0767	15.93	13.56
0.125	0.0291	0.0838	13.96	11.87
0.101	0.0318	0.0915	15.22	13.52
0.088	0.0319	0.0920	14.28	12.81

TABLE II - CONTINUED

Model III: 1.0 inch diameter 45° Cone No Afterbody

V_∞ = 30 fps

σ	Q (cfs)	C_Q	P_∞ (psia)	P_C (psia)
0.283	0.0029	0.0140	16.65	15.21
0.231	0.0082	0.0395	18.00	16.60
0.183	0.0106	0.0510	17.96	16.86
0.153	0.0105	0.0506	16.68	15.76
0.139	0.0116	0.0558	16.50	15.66
0.075	0.0142	0.0680	15.42	14.97

TABLE II - CONTINUED

Model III: 1.0 inch Diameter 45° Cone No Afterbody

V_∞ = 45 fps

σ	Q (cfs)	C_Q	P_∞ (psia)	P_C (psia)
0.291	0.0030	0.0097	22.48	18.52
0.203	0.0130	0.0417	21.80	19.04
0.150	0.0173	0.0554	18.50	16.45
0.141	0.0193	0.0616	17.81	15.89
0.115	0.0231	0.0739	18.93	17.37
0.094	0.0244	0.0781	21.51	16.81

TABLE II - CONTINUED

Model III: 1.0 inch Diameter 45° Cone No Afterbody

V_∞ = 50 fps

σ	Q (cfs)	C_Q	P_∞ (psia)	P_C (psia)
0.292	0.0032	0.0092	19.01	14.11
0.203	0.0146	0.0420	18.45	15.05
0.154	0.0203	0.0585	22.22	19.64
0.144	0.0225	0.0648	20.36	17.94
0.103	0.0257	0.0740	17.25	15.52
0.092	0.0264	0.0761	16.76	15.22
0.066	0.0280	0.0805	14.15	13.04

December 3, 1979
DRS:JWH:cac

TABLE III

Tabulation of Pressure Distribution Data for 45° Cone With the 1.0 inch Afterbody (Model II)

V_∞ = 30 fps

$$C_{P_i} = \frac{P_i - P_\infty}{1/2\rho V_\infty^2}, \quad i=1, 2, \ldots 9$$

where i denotes the pressure tap number

C_{P_i} \ L/D	0	1	4	9
C_{P1}	0.390	0.418	0.426	0.496
C_{P2}	0.290	0.322	0.334	0.404
C_{P3}	0.234	0.263	0.283	0.366
C_{P4}	0.171	0.197	0.220	0.297
C_{P5}	0.079	0.121	0.158	0.225
C_{P6}	-0.051	0.024	0.089	0.155
C_{P7}	-0.383	-0.198	-0.079	0.004
C_{P8}	-0.153	-0.378	-0.170	-0.082
C_{P9}	-0.085	-0.365	-0.170	-0.090

TABLE III - CONTINUED

V_∞ = 45 fps

C_{P_i} \ L/D	0	1	4	6	10
C_{P1}	0.417	0.411	0.436	0.438	0.464
C_{P2}	0.304	0.306	0.344	0.350	0.368
C_{P3}	0.249	0.255	0.298	0.312	0.329
C_{P4}	0.174	0.194	0.238	0.255	0.274
C_{P5}	0.082	0.118	0.175	0.205	0.218
C_{P6}	-0.051	0.013	0.098	0.125	0.145
C_{P7}	-0.390	-0.210	-0.079	-0.028	-0.010
C_{P8}	-0.164	-0.404	-0.161	-0.112	-0.003
C_{P9}	-0.081	-0.369	-0.156	-0.115	-0.066

TABLE III - CONTINUED

V_∞ = 50 fps

C_{P_i} \ L/D	0	1	4	6	8	10
C_{P1}	0.403	0.416	0.425	0.448	0.479	0.453
C_{P2}	0.297	0.313	0.328	0.350	0.388	0.352
C_{P3}	0.237	0.261	0.287	0.306	0.347	0.323
C_{P4}	0.168	0.196	0.234	0.253	0.289	0.270
C_{P5}	0.076	0.118	0.174	0.204	0.229	0.202
C_{P6}	-0.055	0.016	0.091	0.117	0.155	0.132
C_{P7}	-0.399	-0.207	-0.091	-0.032	0.001	-0.023
C_{P8}	-0.169	-0.401	-0.168	-0.121	-0.076	-0.095
C_{P9}	-0.083	-0.361	-0.170	-0.124	-0.072	-0.094

TABLE IV

Tabulation of Pressure Tap Locations For
45° Cone With the 1.0 inch Afterbody (Model II)

Tap / Distance S (inch)	1	2	3	4	5	6	7	8	9
Present Model	0.180	0.452	0.634	0.778	0.933	1.080	1.232	1.596	1.810
Kim and Holl's Model	0.200	0.470	0.650	0.800	0.945	1.100	1.250	1.612	1.812

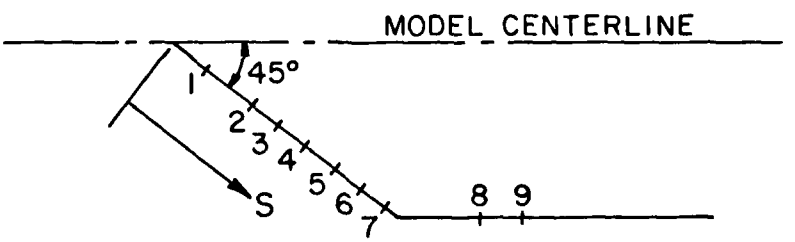

TABLE V

DESCRIPTION OF THE TRANSITION BETWEEN THE REENTRANT JET AND TWIN VORTEX REGIMES FOR VELOCITIES OF 30, 45, AND 50 fps (MODEL III)

V_∞ = 30 fps

1. The cavity length was increased to L/D=5.5 (C_Q=0.0582, σ^*=0.146).
2. A small increase in the air flowrate and the cavity grew to L/D=25.
3. The flowrate was decreased to C_Q=0.0352 without any significant change in cavity length.
4. A further decrease in the flowrate and the cavity decreased in length to L/D=2.5.

V_∞ = 45 fps

1. The cavity length was increased to L/D=7.5 (C_Q=0.0751, σ^*=0.115).
2. A small increase in the air flowrate and the cavity grew to L/D=25.
3. The flowrate was decreased to C_Q=0.0563 without any significant change in cavity length.
4. A further decrease in the flowrate and the cavity decreased in length to L/D=5.

V_∞ = 50 fps

1. The cavity length was increased to L/D=8.5 (C_Q=0.0743, σ^*=0.100)
2. A small increase in the air flowrate and the cavity grew to L/D=25.
3. The flowrate was decreased to C_Q=0.0610 without any significant change in cavity length.
4. A further decrease in the flowrate and the cavity decreased in length to L/D=5.

NOTE: σ^* is defined as the lowest possible σ which can be attained before transition to the twin vortex regime occurs.

December 3, 1979
DRS:JWH:cac

TABLE VI

TABULATION OF INSTANTANEOUS CAVITATION NUMBER AND CAVITY LENGTH FOR THE CAVITY ATTRITION TESTS (MODEL III)

Test 4	Frame	L/D	σ_p
50 fps	1	4.4	0.80
Framing rate - 17.5pps	2	4.4	0.107
	3	4.4	0.102
	4	4.4	0.107
	5	4.3	0.103
	6	3.8	0.089
	7	2.7	0.131
	8	2.0	0.182
	9	1.7	0.257
Test 5	1	7.3	0.125
50 fps	2	7.0	0.104
Framing rate - 17.4pps	3	6.6	0.100
	4	6.3	0.114
	5	5.5	0.132
	6	3.8	0.163
	7	2.9	0.191
	8	1.9	0.228
	9	1.7	0.287
Test 6	1	8.3	0.94
50 fps	2	9.2	0.115
Framing rate - 17.4pps	3	8.4	0.125
	4	7.6	0.116
	5	6.2	0.127
	6	4.4	0.157
	7	3.1	0.171
	8	2.4	0.208
	9	1.7	0.263
Test 7	1	4.9	0.129
30 fps	2	4.8	0.172
Framing rate - 17.4pps	3	4.8	0.183
	4	4.1	0.183
	5	3.3	0.184
	6	2.8	0.252
	7	1.8	0.247
	8	1.6	0.309
	9	1.6	0.362

Test 8	Frame	L/D	σ_p
30 fps	1-40	>10	———
Framing rate - 17.4pps	41	9.8	0.112
(Starting in Twin	42	9.8	0.119
Vortex Regime)	43	8.9	0.126
	44	8.3	0.126
	45	8.9	0.119
	46	7.4	0.122
	47	6.8	0.123
	48	6.7	0.124
	49	6.5	0.131
	50	5.9	0.140
	51	5.8	0.150
	52	5.5	0.143
	53	4.8	0.154
	54	4.8	0.158
	55	4.1	0.169
	56	3.7	0.164
	57	——	0.181
	58	2.0	0.229
	59	——	0.297
	60	1.4	0.246
Test 10	1-14	>10	———
50 fps	15	10.2	0.07
Framing rate - 17.4pps	16	8.4	0.08
(Starting in Twin	17	6.7	0.08
Vortex Regime)	18	5.0	0.10
	19	4.1	0.13
	20	2.2	0.14
	21	1.8	0.21
	22	1.6	0.21
Test 14	1	7.1	0.103
50 fps	2	6.8	0.114
Framing rate - 21.6pps	3	6.7	0.118
	4	6.0	0.109
	5	4.6	0.103
	6	3.8	0.113
	7	2.9	0.138
	8	1.8	0.172
	9	1.5	0.183
	10	1.3	0.240

December 3, 1970
DRS:JWH:cac

TABLE VI - CONTINUED

	Frame	L/D	σ_p
Test 15	1-16	>10	———
50 fps	17	10	0.063
Framing rate-21.6pps	18	8.9	0.065
(Starting in Twin	19	7.1	0.068
Vortex Regime)	20	5.7	0.068
	21	4.9	0.066
	22	3.8	0.069
	23	2.9	0.083
	24	2.1	0.091
	25	1.6	0.114
Test 16	1	5.6	0.117
30 fps	2	5.5	0.152
Framing rate-21.6pps	3	5.2	0.107
	4	4.3	0.127
	5	4.1	0.132
	6	3.2	0.133
	7	2.7	0.124
	8	2.3	0.162
	9	2.0	0.162
	10	1.7	0.200
Test 17	1-41	>10	———
30 fps	42	10.3	0.057
Framing rate-21.6pps	43	9.8	0.047
(Starting in Twin	44	9.1	0.047
Vortex Regime)	45	9.1	0.047
	46	9.1	0.042
	47	8.7	0.042
	48	8.0	0.040
	49	8.0	0.053
	50	7.2	0.047
	51	7.2	0.048
	52	6.8	0.042
	53	6.3	0.049
	54	5.9	0.063
	55	5.7	0.069
	56	5.0	0.066
	57	4.3	0.058
	58	4.3	0.051
	59	3.8	0.054
	60	2.9	0.053
	61	2.3	0.059
	62	1.8	0.045
	63	1.8	0.053
	64	1.5	0.073
Test 18	1-16	>10	———
50 fps	17	9.7	0.037
Framing rate-21.6pps	18	8.6	0.049
(Starting in Twin	19	7.2	0.050
Vortex Regime)	20	5.8	0.061
	21	4.3	0.046
	22	3.3	0.072
	23	2.2	0.079
	24	1.7	0.079
Test 19	1	6.8	0.129
50 fps	2	5.4	0.130
Framing rate-21.6pps	3	4.1	0.112
	4	3.5	0.137
	5	2.6	0.133
	6	1.7	0.186
	7	1.5	0.287
	8	1.4	0.318
	9	——	0.338

TABLE VI - CONTINUED

Cavity Attrition Tests - Ventilation Air Only Turned Off (Tunnel Running)

All 50fps - Framing rate = 21.6pps

	Frame	L/D	σ_v
Test 24	1	8.6	0.122
	2	6.4	0.121
	3	5.5	0.122
	4	3.8	0.169
	5	2.9	0.162
	6	2.2	0.183
	7	1.5	0.216
	8	1.4	0.342
	9	——	0.383
Test 25	1	9.5	0.152
	2	9.3	0.193
	3	9.2	0.216
	4	7.6	0.171
	5	5.7	0.214
	6	4.1	0.252
	7	2.9	0.253
	8	1.9	0.255
	9	1.4	0.329
	10	——	0.442
Test 26 (Starting in Twin Vortex Regime)	1-18	>10	———
	19	10.4	0.087
	20	9.1	0.071
	21	7.9	0.094
	22	6.9	0.094
	23	5.5	0.094
	24	4.3	0.118
	25	3.3	0.114
	26	2.5	0.135
	27	1.9	0.145
	28	——	0.148
Test 27	1	10.4	0.109
	2	9.7	0.097
	3	9.1	0.110
	4	7.9	0.110
	5	7.0	0.121
	6	6.3	0.140
	7	3.8	0.142
	8	2.8	0.144
	9	2.4	0.211
	10	1.8	0.247
Test 28 (Starting in Twin Vortex Regime)	1-17	>10	———
	18	11.3	0.074
	19	10.5	0.082
	20	9.3	0.084
	21	8.1	0.081
	22	6.3	0.086
	23	5.0	0.100
	24	4.0	0.114
	25	2.8	0.127
	26	1.9	0.133
	27	1.0	0.150
	28	——	0.164
Test 29	1	10.1	0.116
	2	8.9	0.118
	3	7.5	0.110
	4	6.7	0.100
	5	5.1	0.115
	6	3.8	0.141
	7	3.0	0.159
	8	1.9	0.184
	9	1.8	0.233
	10	——	0.288
Test 30	1	7.5	0.109
	2	5.8	0.113
	3	5.2	0.131
	4	3.3	0.147
	5	2.3	0.176
	6	1.8	0.196
	7	——	0.297

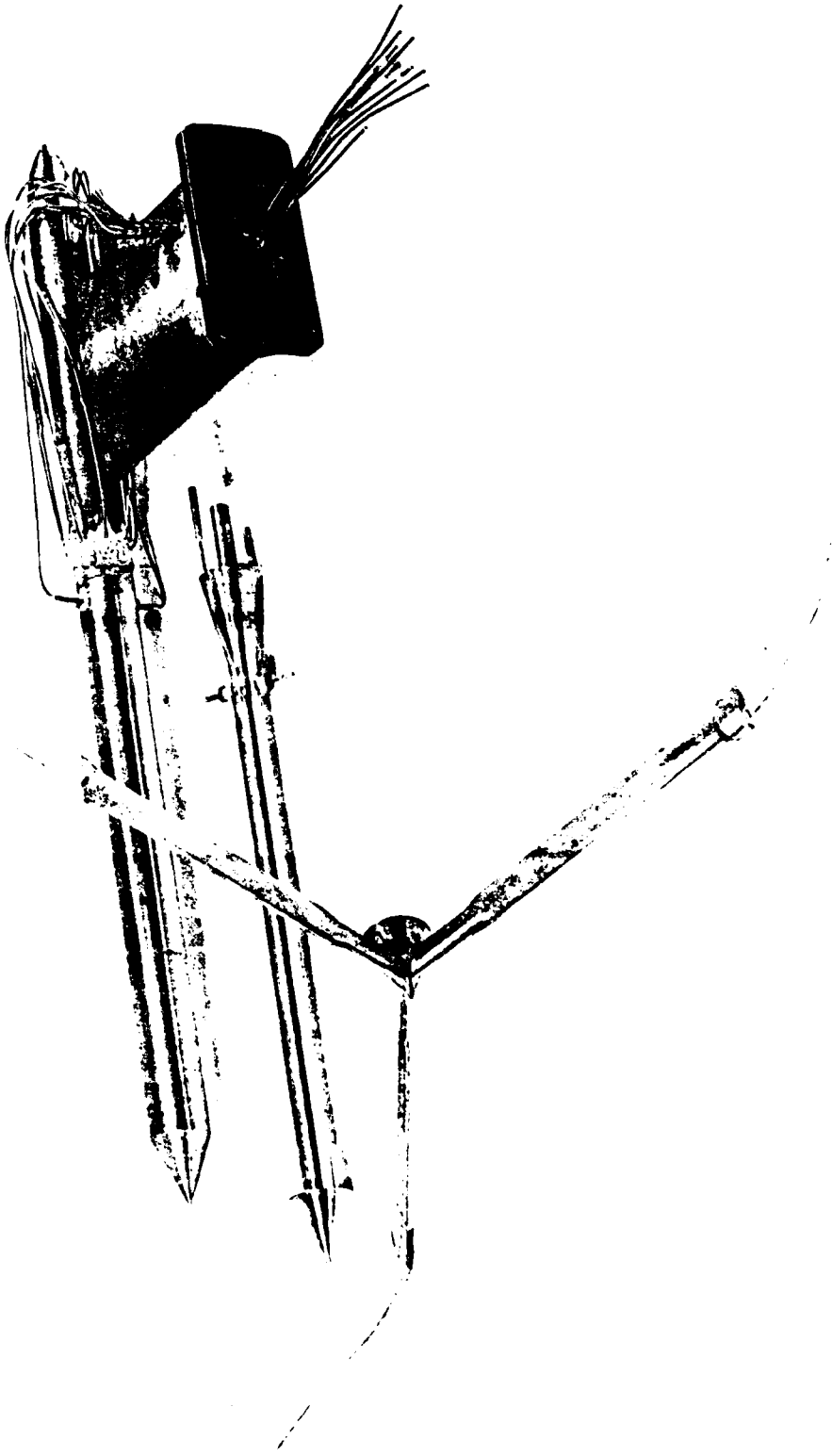

December 3, 1979
DRS:JWH:cac

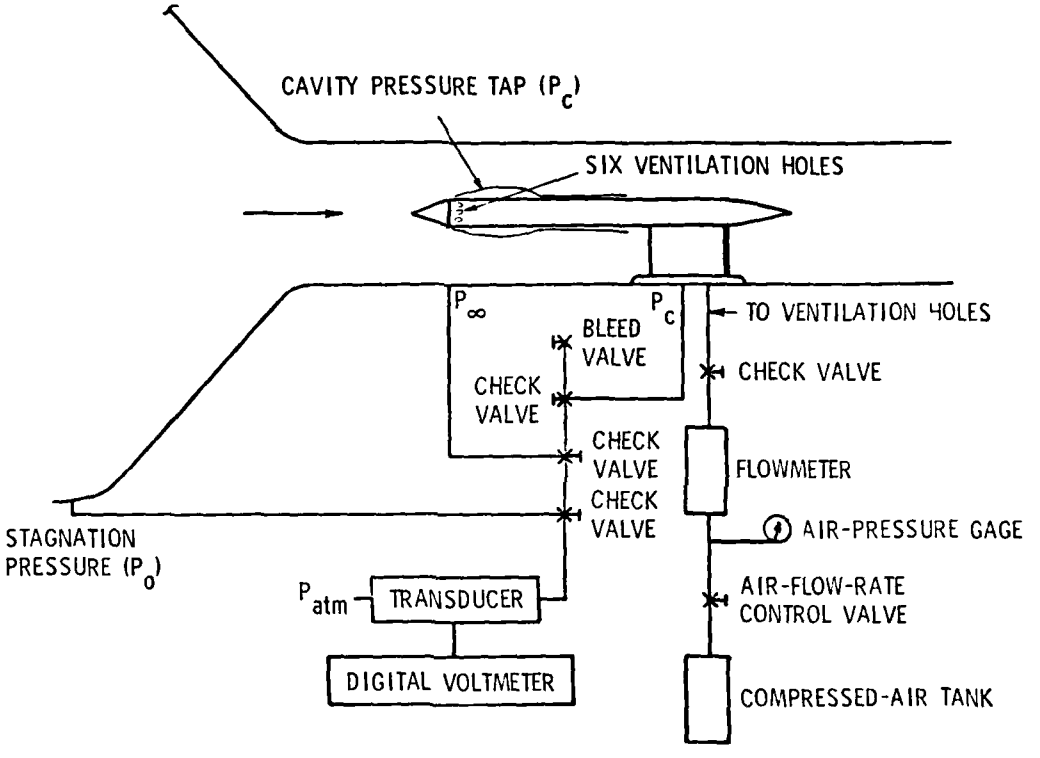

Figure 2 - Sketch of Test Arrangement for Steady State Measurements

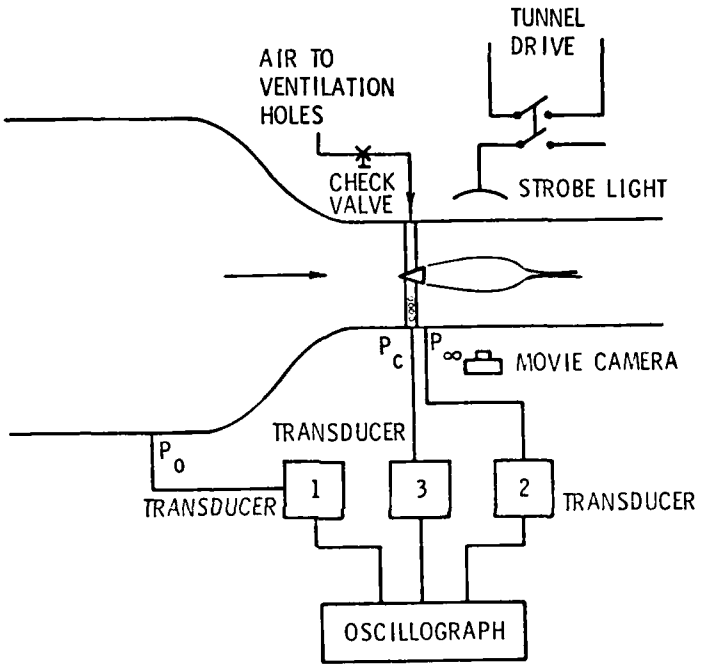

Figure 3 - Sketch of Test Arrangement for Cavity Attrition Tests

December 3, 1979
DRS:JWH:cac

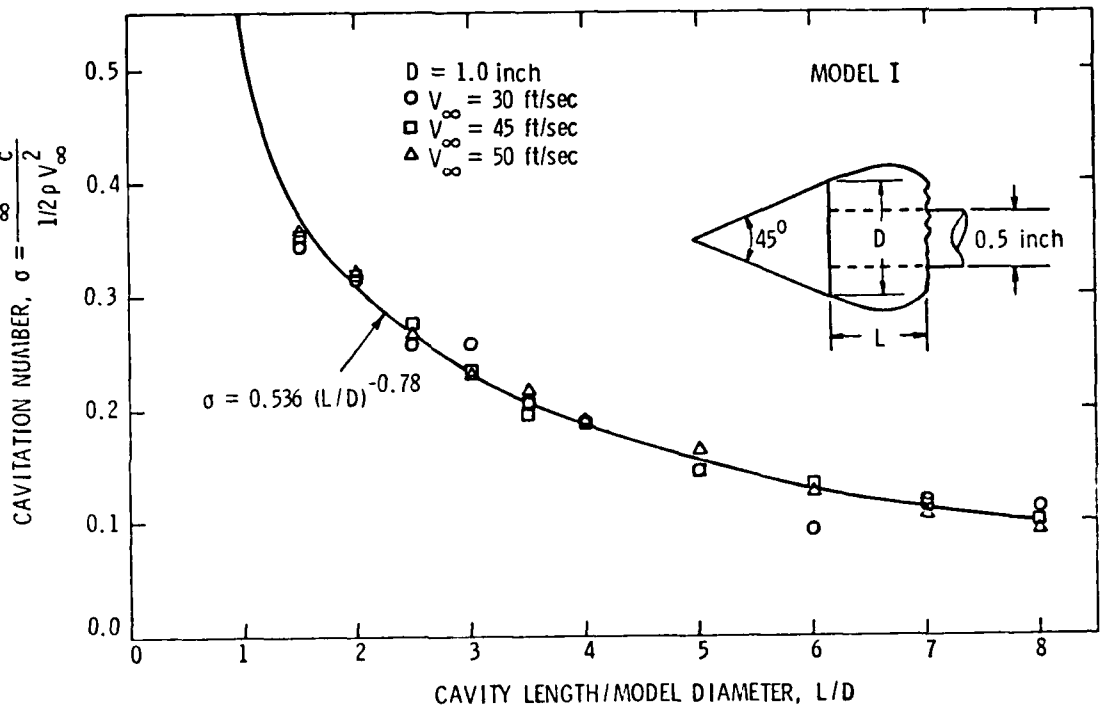

Figure 4 - Cavitation Number Versus Cavity Length for 1.0 inch Diameter, 45° Conical Head Model with a 0.5 inch Diameter Afterbody (Model I)

December 3, 1979
DRS:JWH:cac

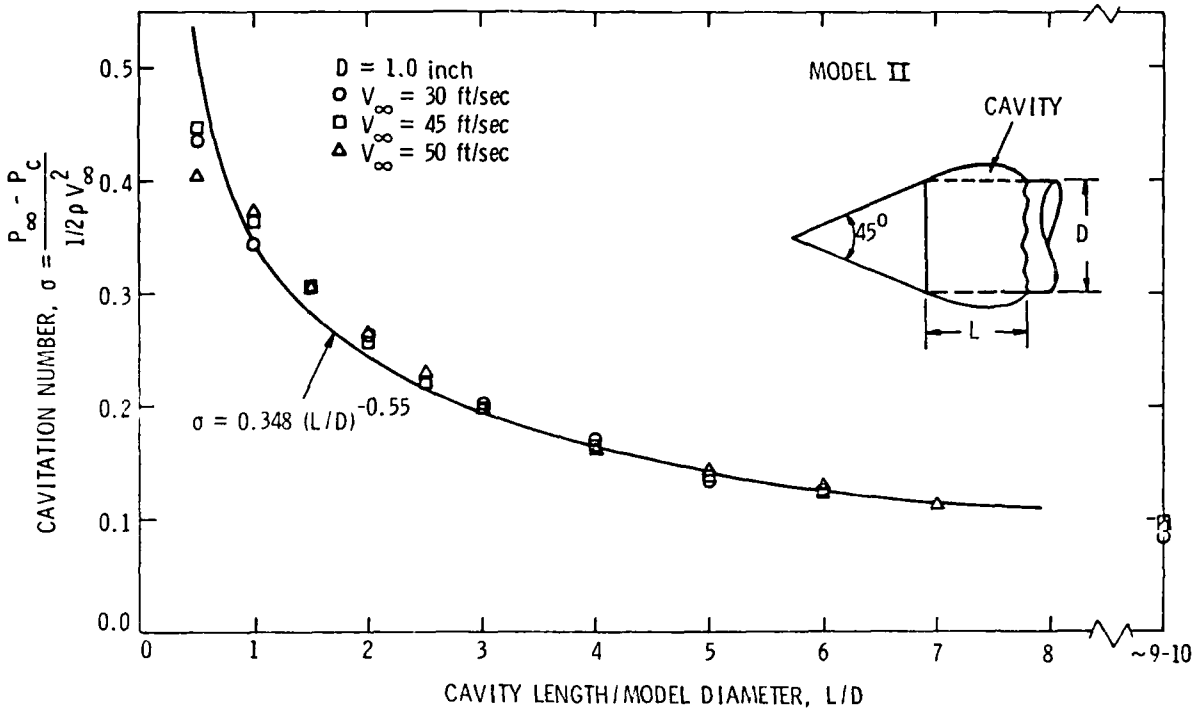

Figure 5 - Cavitation Number Versus Cavity Length for 1.0 inch Diameter, 45° Conical Head Model with a 1.0 inch Diameter Afterbody (Model II)

December 3, 1979
DRS:JWH:cac

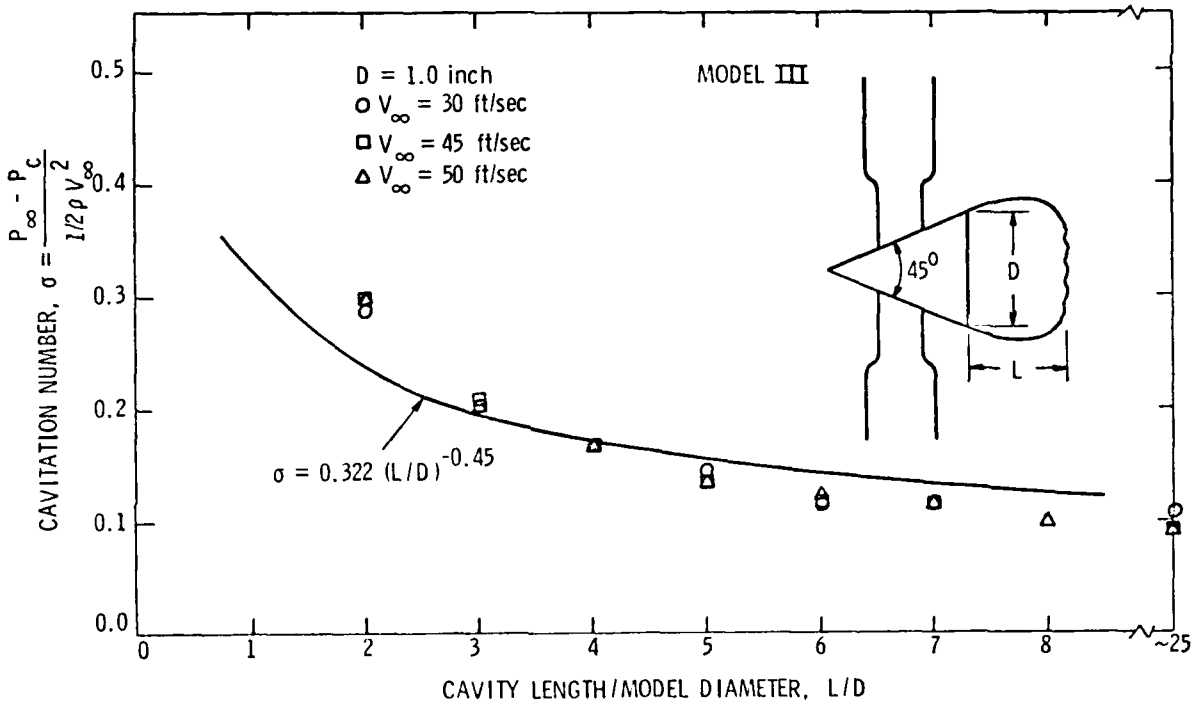

Figure 6 - Cavitation Number Versus Cavity Length for 1.0 inch Diameter, 45° Conical Head Model with No Afterbody (Model III)

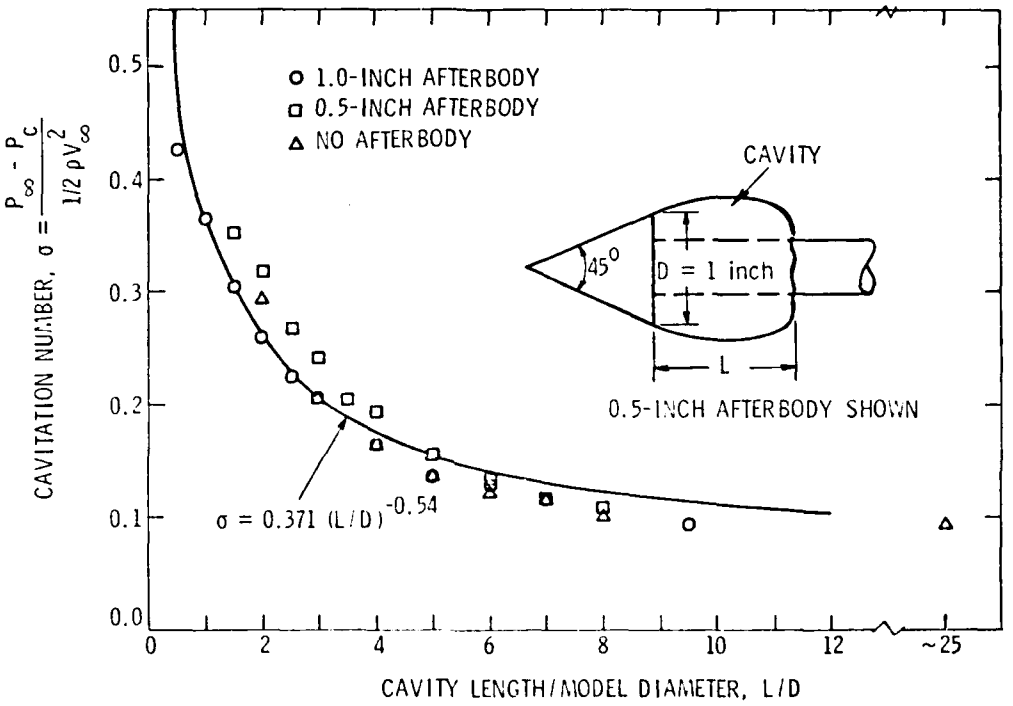

Figure 7 - Cavitation Number Versus Cavity Length for 1.0 inch Diameter, 45° Conical Head Models

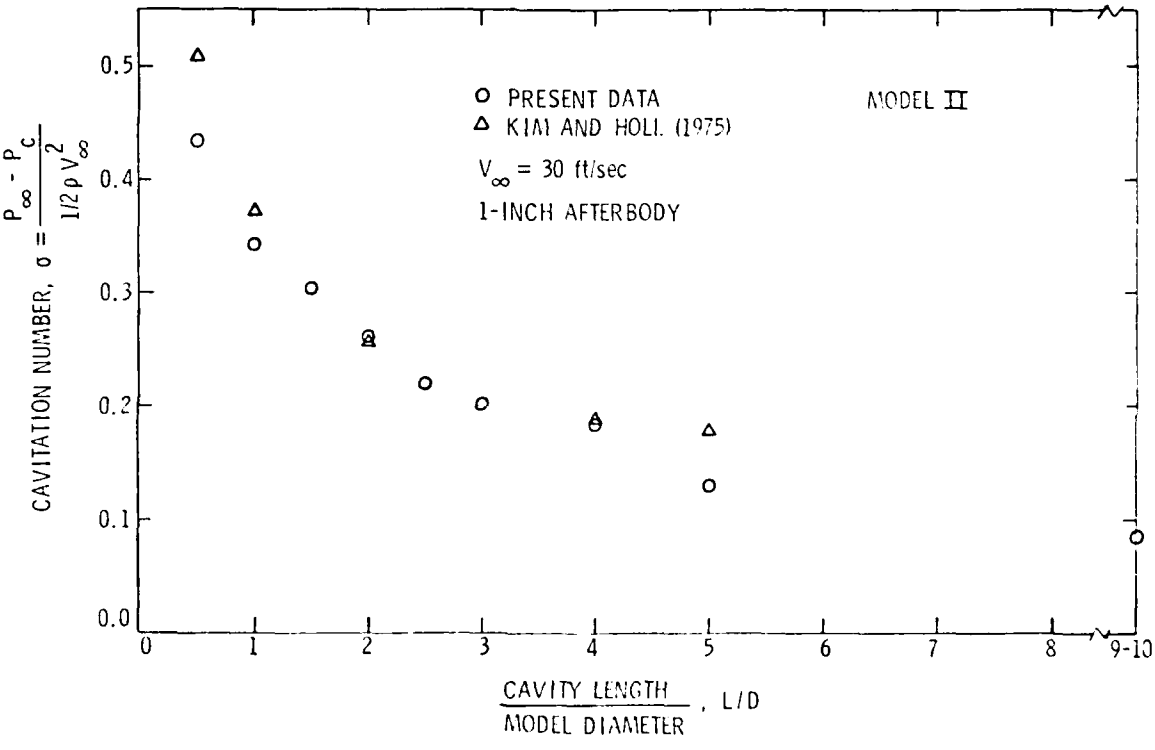

Figure 8 - Cavitation Number Versus Cavity Length for 1.0 inch Diameter, 45° Conical Head Models with 1.0 inch Diameter Afterbodies - Comparison with the Results of Kim and Holl (1975), V_∞ = 30 ft/sec

December 3, 1979
DRS:JWH:cac

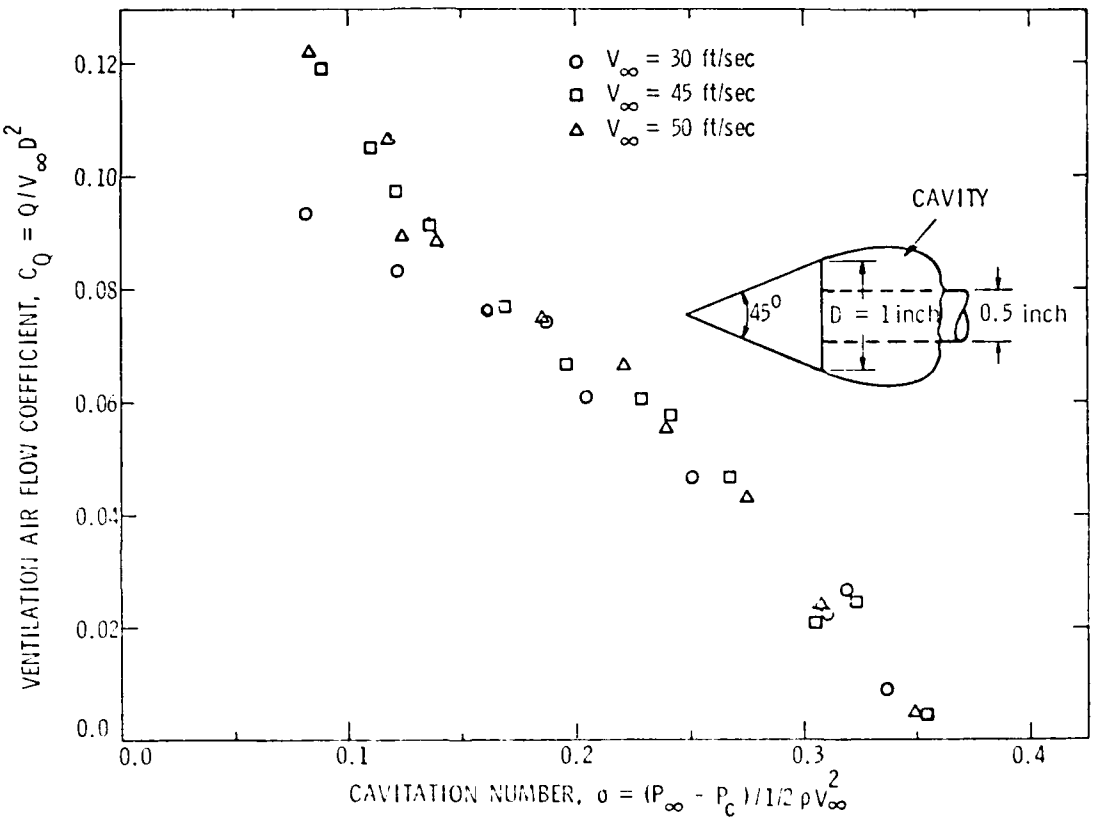

Figure 9 - Ventilation Air Flow Coefficient Versus Cavitation Number for 1.0 inch Diameter, 45° Conical Head Model with a 0.5 inch Diameter Afterbody (Model I)

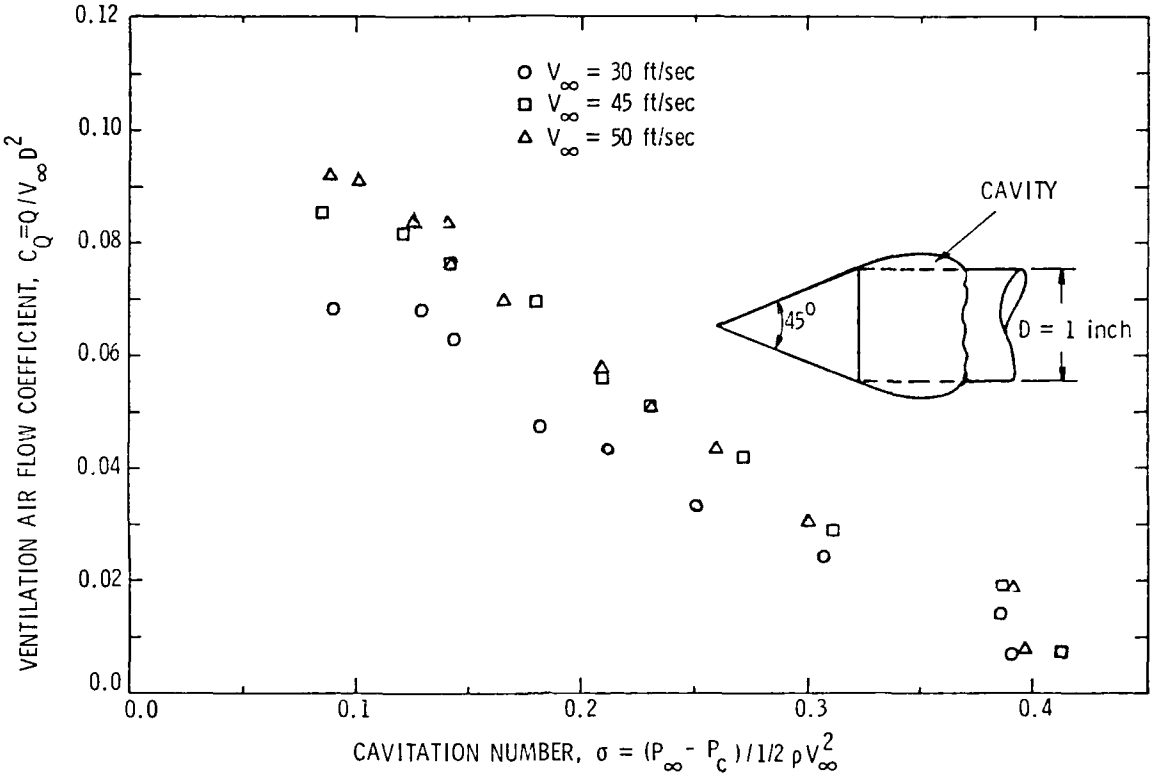

Figure 10 - Ventilation Air Flow Coefficient Versus Cavitation Number for 1.0 inch Diameter, 45° Conical Head Model with a 1.0 inch Diameter Afterbody (Model II)

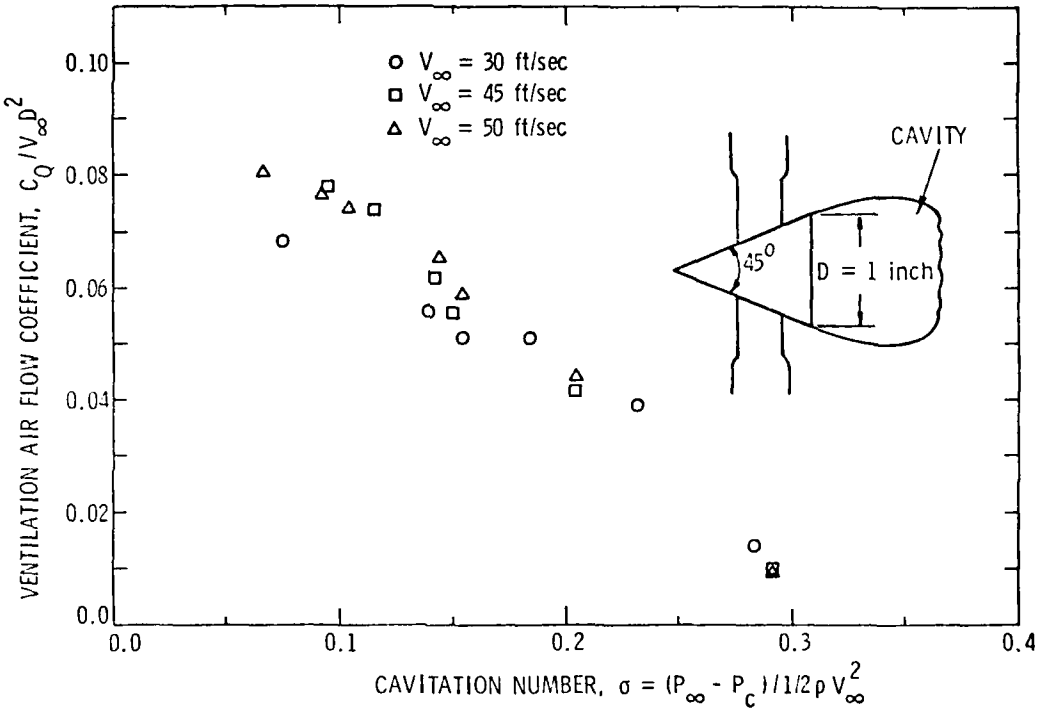

Figure 11 - Ventilation Air Flow Coefficient Versus Cavitation Number for 1.0 inch Diameter, 45° Conical Head Model with No Afterbody (Model III)

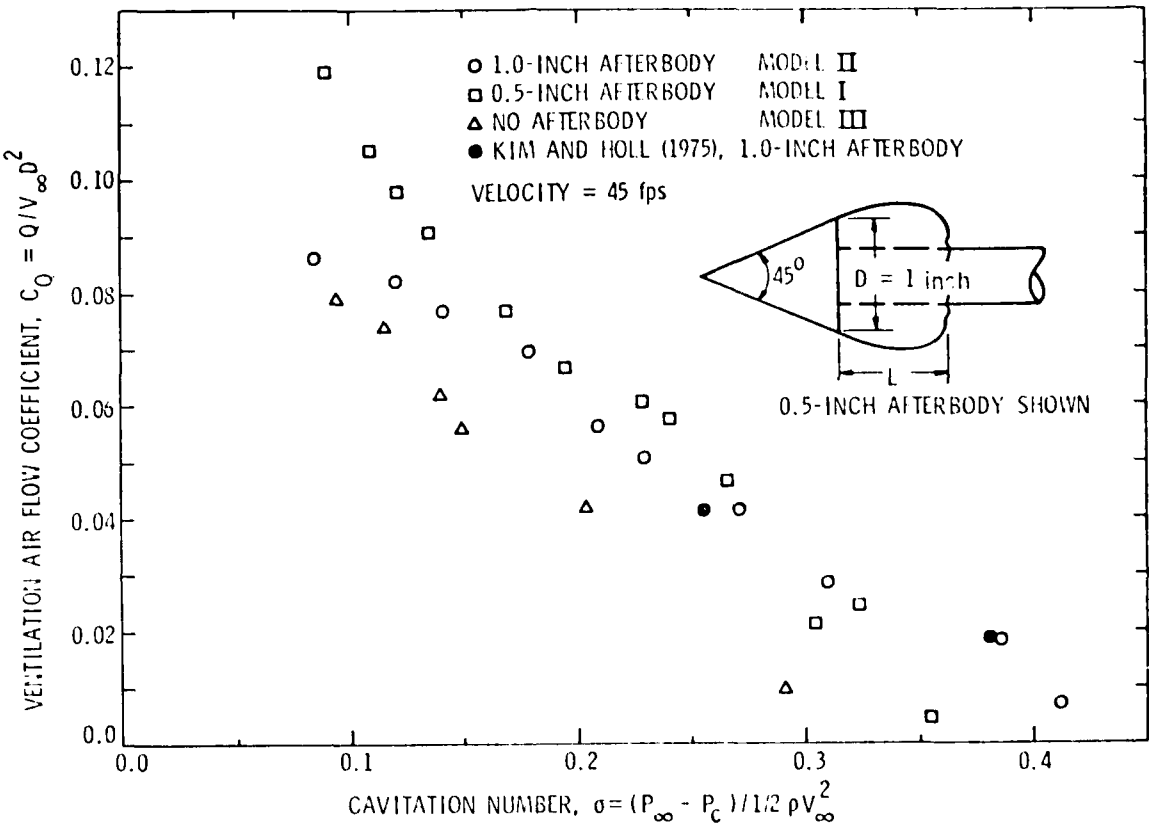

Figure 12 - Ventilation Air Flow Coefficient Versus Cavitation Number for 1.0 inch Diameter, 45° Conical Head Models

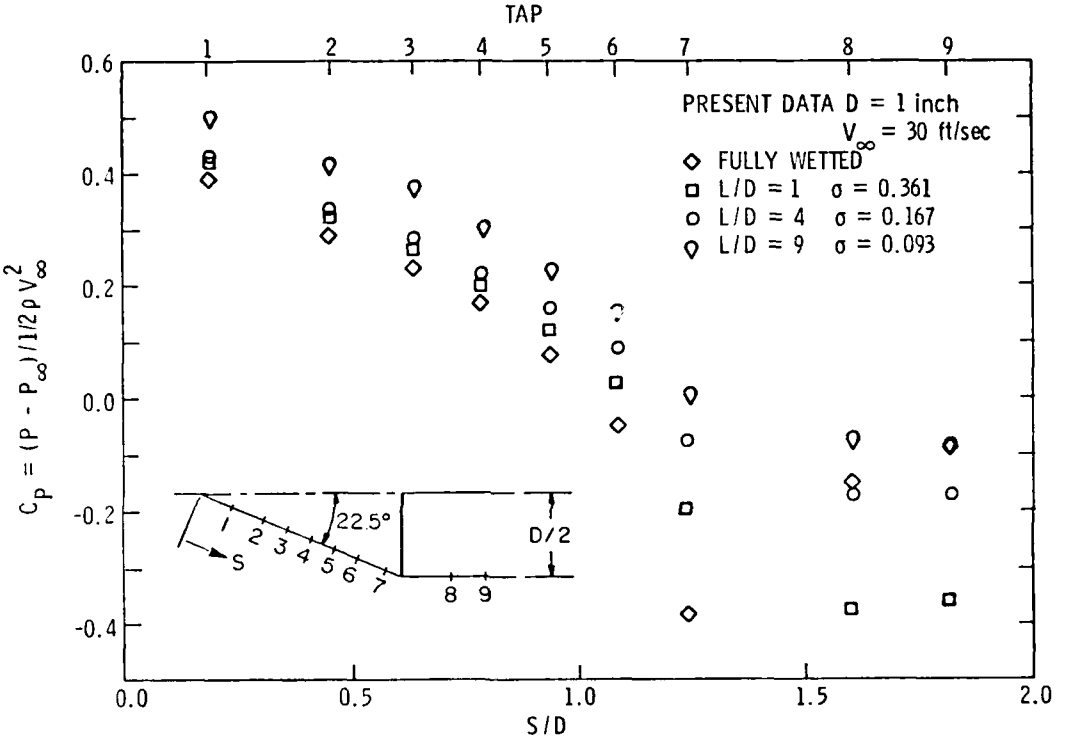

Figure 13 - Local Pressure Coefficient Along the Body Surface of 1.0 inch Diameter, 45° Conical Head Model with a 1.0 inch Diameter Afterbody, (Model II) - V_∞ = 30 ft/sec

December 3, 1979
DRS:JWH:cac

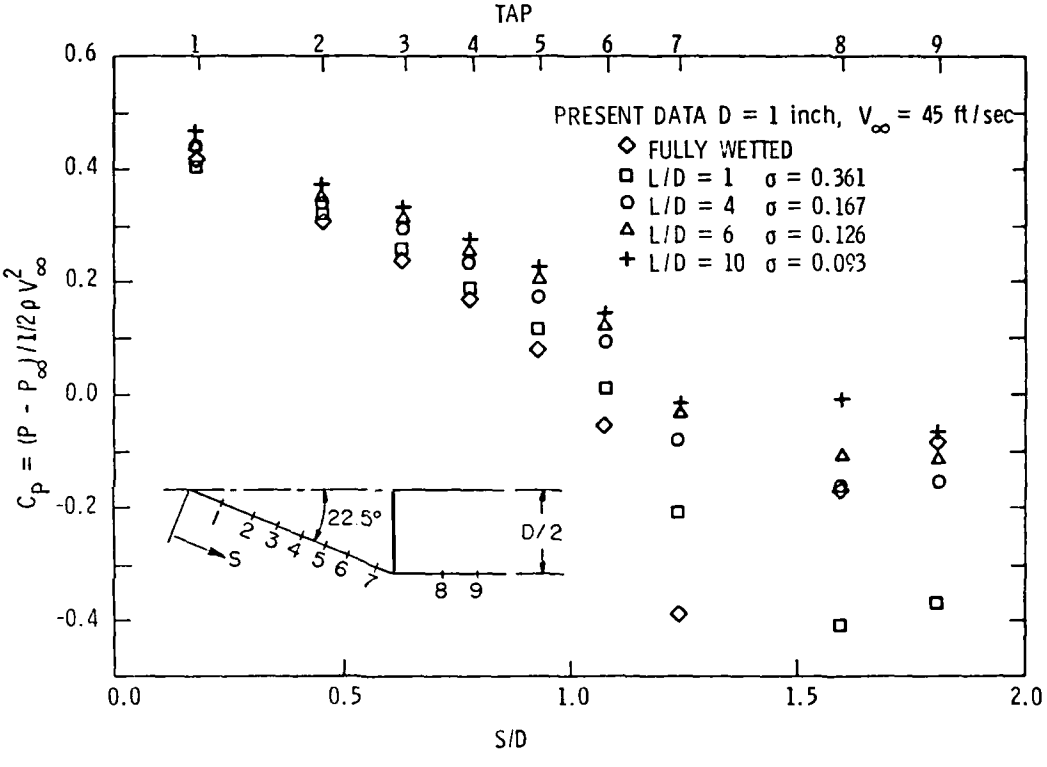

Figure 14 - Local Pressure Coefficient Along the Body Surface for 1.0 inch Diameter, 45° Conical Head Model with a 1.0 inch Diameter Afterbody (Model II) - V_∞ = 45 ft/sec

December 3, 1979
DRS:JWH:cac

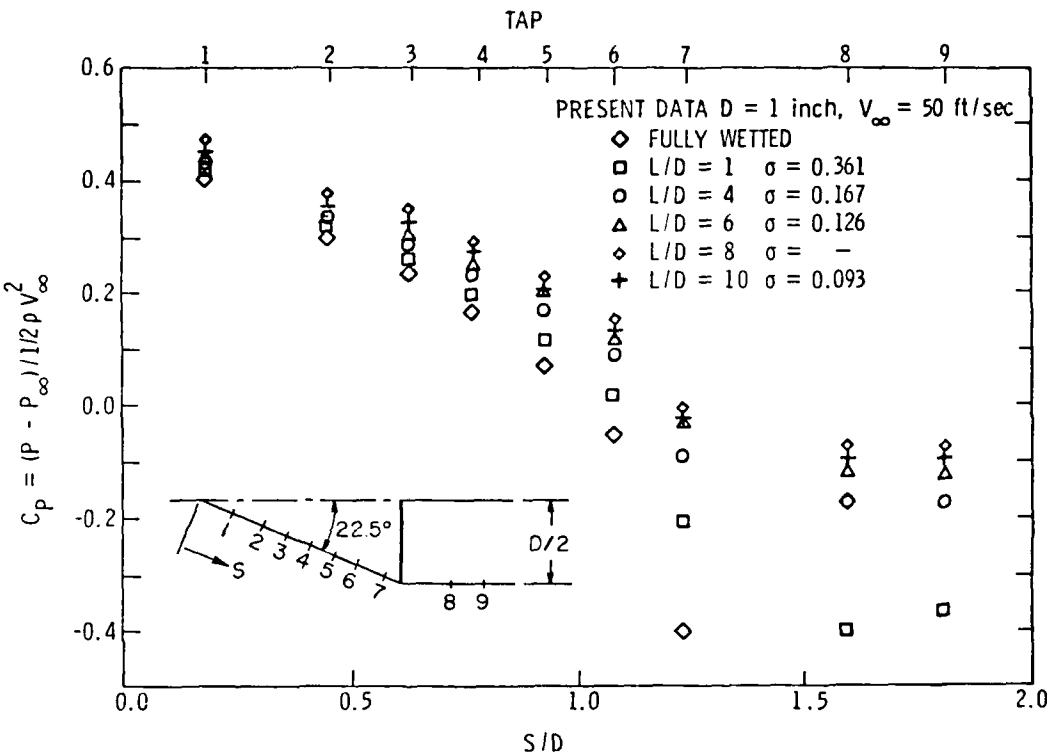

Figure 15 - Local Pressure Coefficient Along the Body Surface for 1.0 inch Diameter, 45° Conical Head Model with a 1.0 inch Diameter Afterbody (Model II) - V_∞ = 50 ft/sec

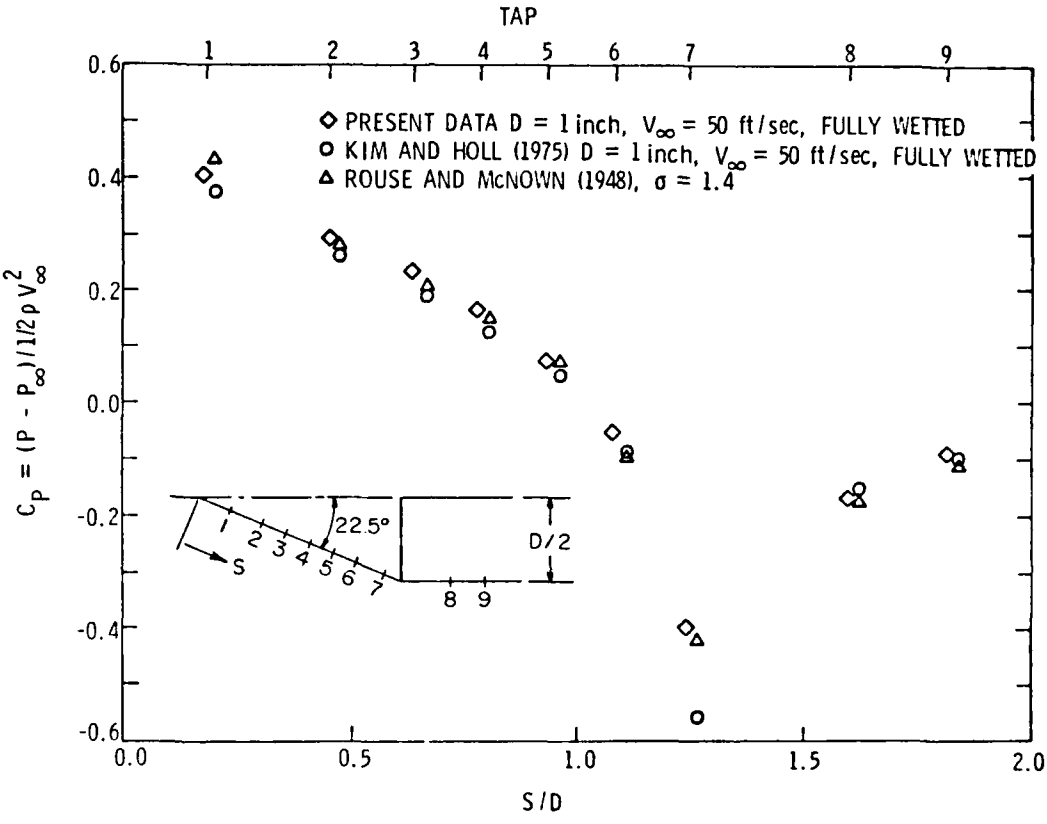

Figure 16 - Local Pressure Coefficient Along the Body Surface for 1.0 inch Diameter, 45° Conical Head Models with 1.0 inch Diameter Afterbodies - Comparison with the Results of Kim and Holl (1975) and Rouse and McNown (1948)

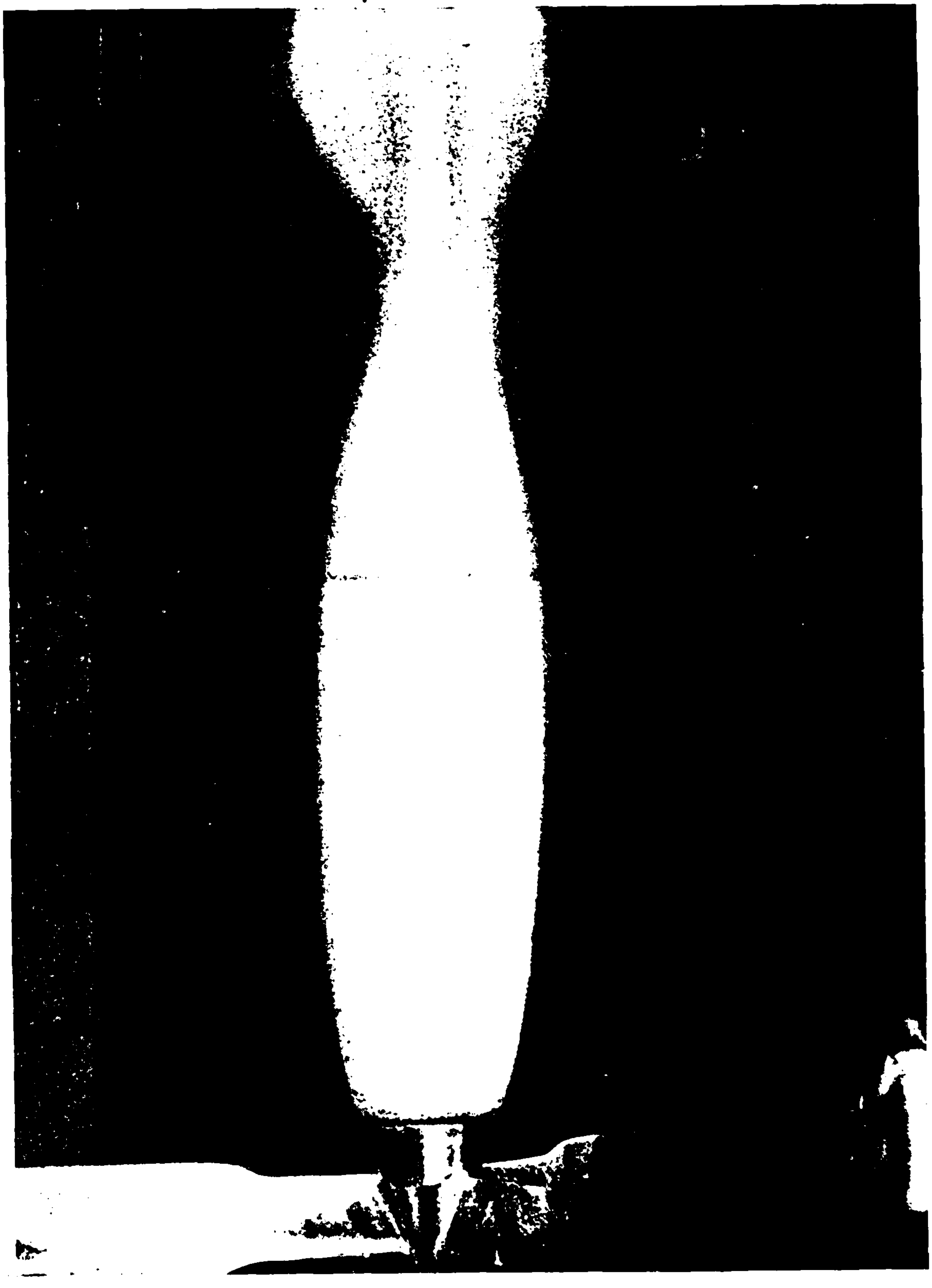

Figure 17 – Photograph of a [illegible] Cavity in the Reentrant Jet Regime, [illegible] L/h = 7 (Model III)

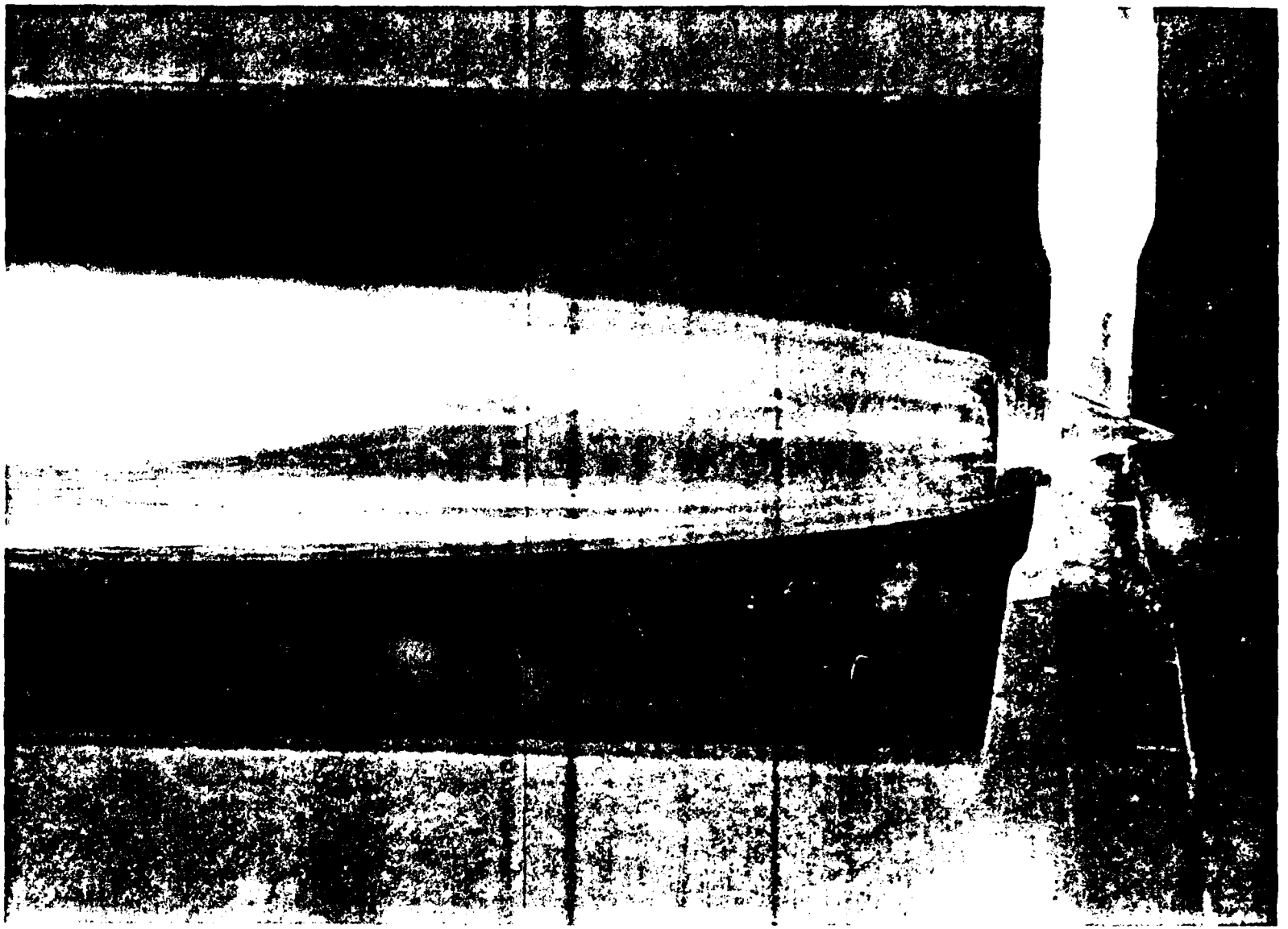

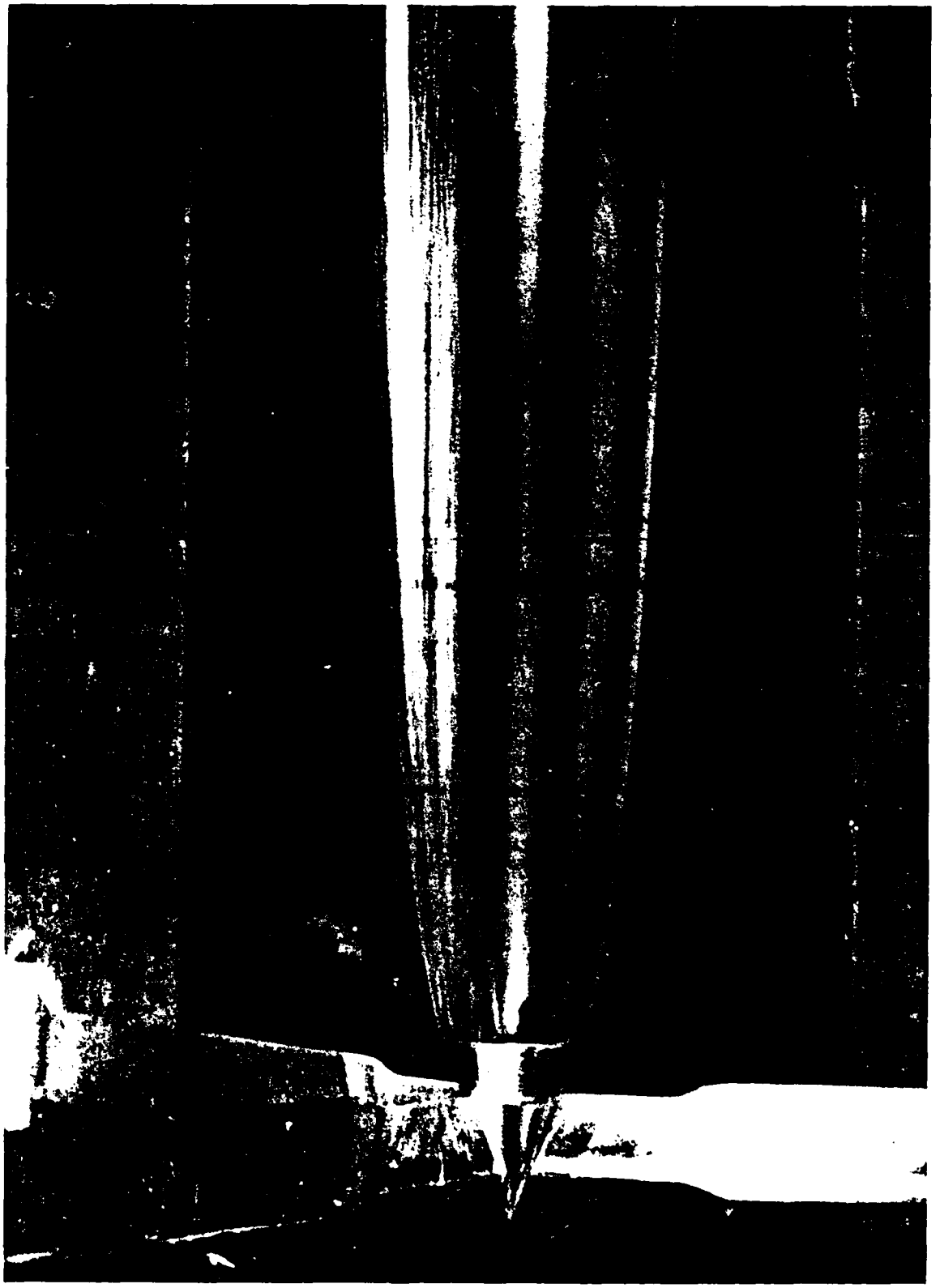

Figure 19 - Photograph of a Confluated Cavity in the Twin Vortex Device.
V_∞ = 30 ft/sec and L/D = 25 (Model III)

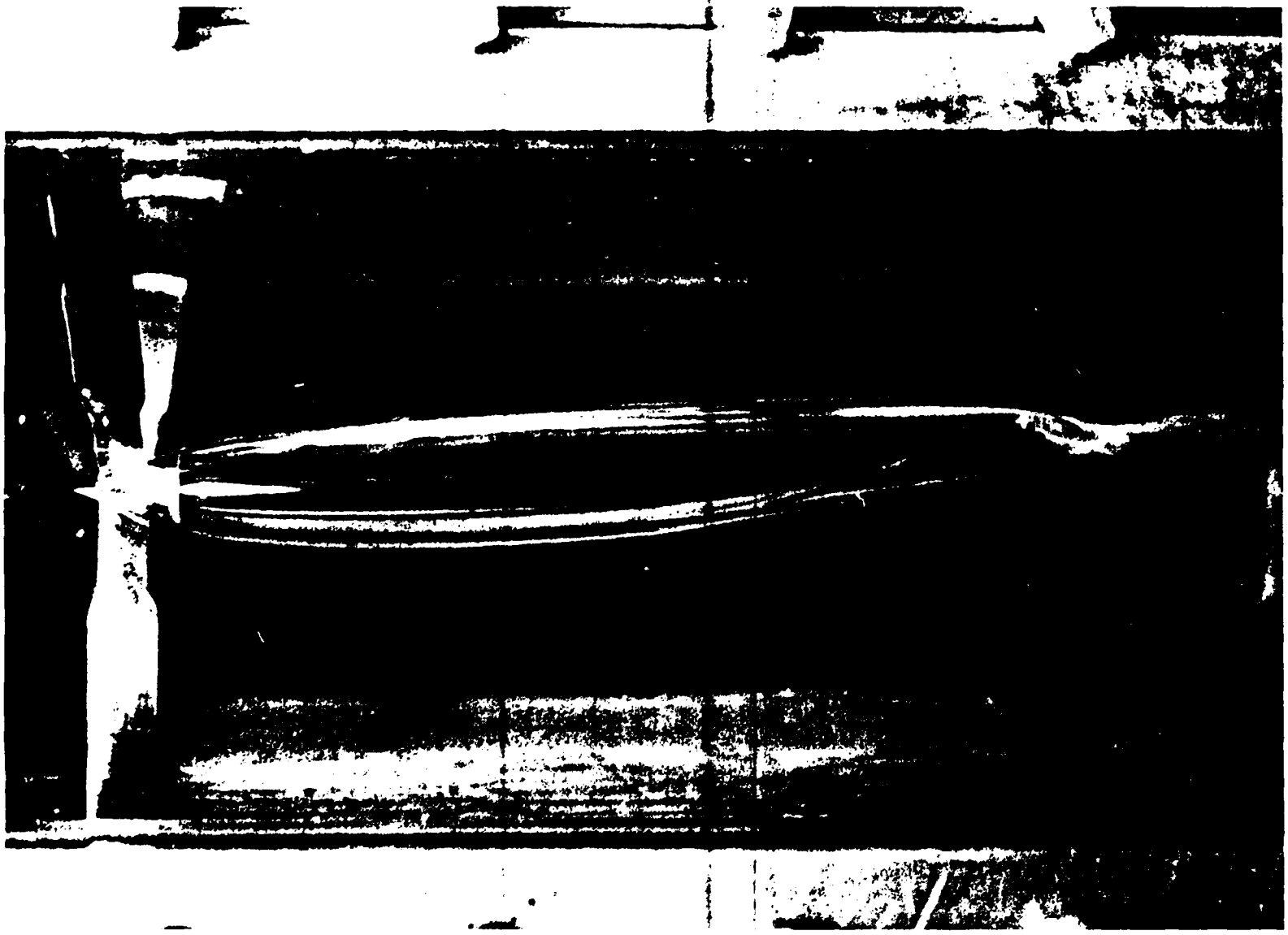

Figure 2[illegible] - Photograph of a Ventilated Cavity in the Twin Vortex Regime, V_∞ = 15 ft/sec and L/L = 11 (Model III)

December 3, 1971
DRSI-[illegible]

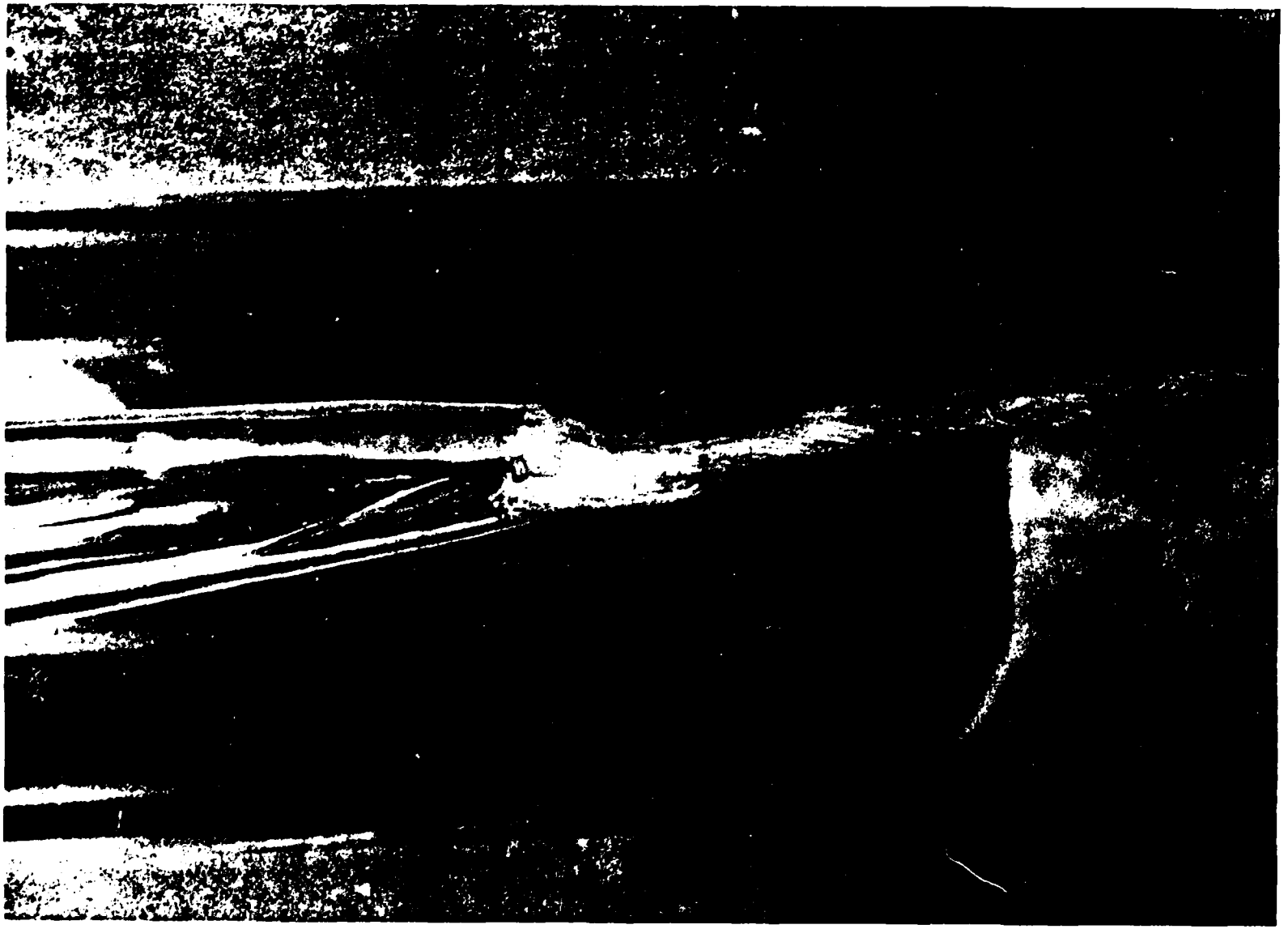

Figure 21 - Detail of Trailing Edge of a Ventilated Cavity in the Twin Vortex Regime, V = 15 ft/sec and L/D = 11 (Model III)

December 3, 1979
DRS:JWH:cac

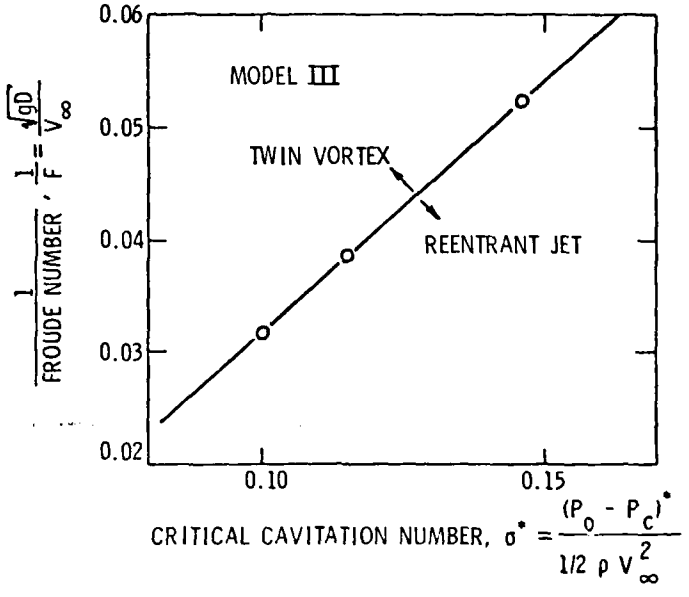

Figure 22 - Influence of Gravity on the Transition of Flow Regimes - 1.0 inch Diameter, 45° Conical Head Body with No Afterbody (Model III)

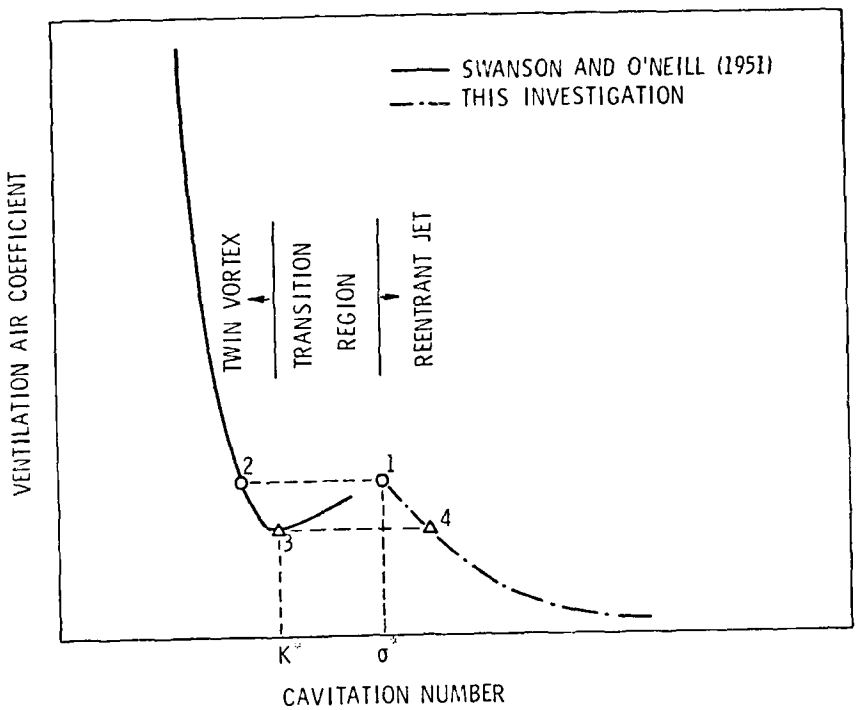

Figure 23 - A Graph Showing the Method for Determining the Critical Cavitation Index, σ*, Together With the Method for Determining k*, as Found by Swanson and O'Neill (1951)

December 3, 1979
DRS:JWH:cac

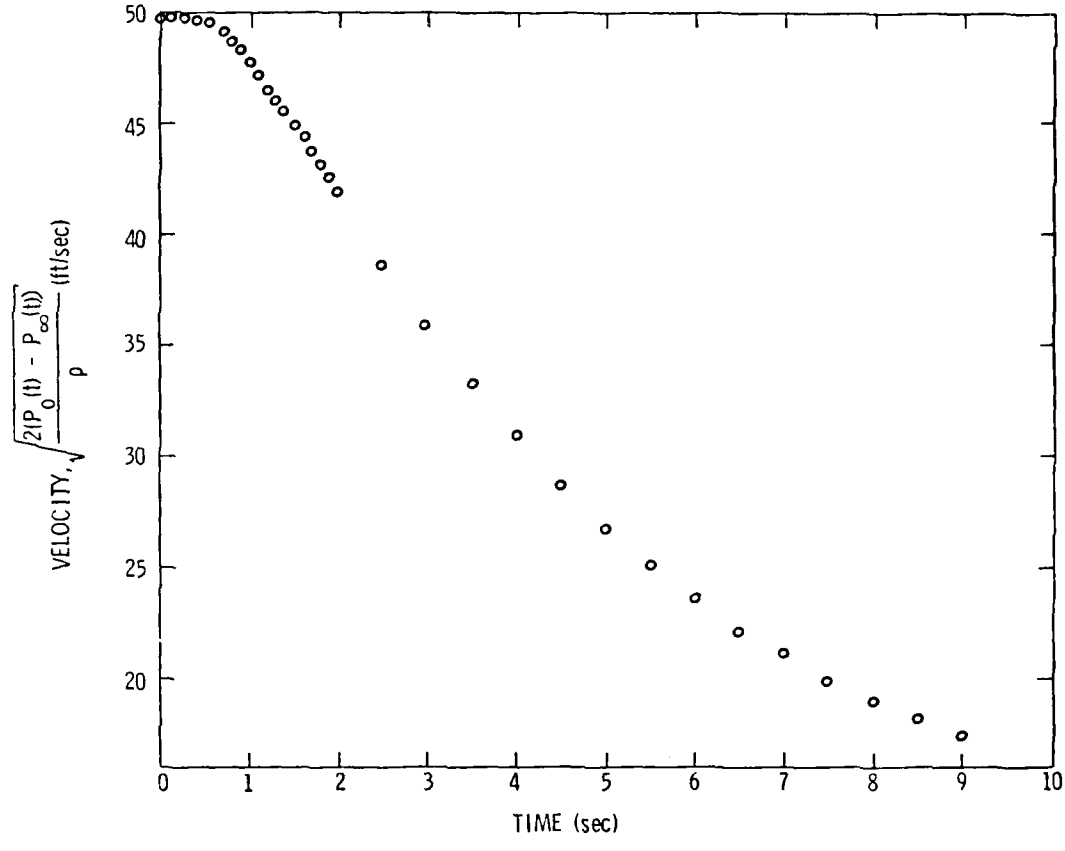

Figure 24 - Graph of Test Velocity as a Function of Time During the Cavity Attrition Tests

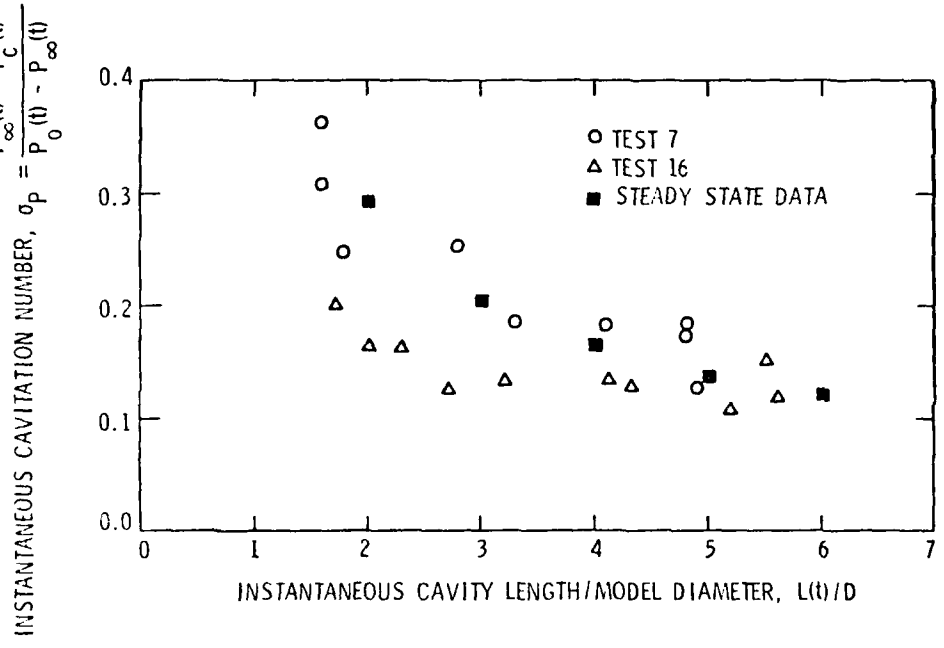

Figure 25 - Instantaneous Cavitation Number, σ_p, Versus Instantaneous Cavity Length for 1.0 inch Diameter, 45° Conical Head Model with No Afterbody (Model III), $V_\infty(0)$ = 30 ft/sec

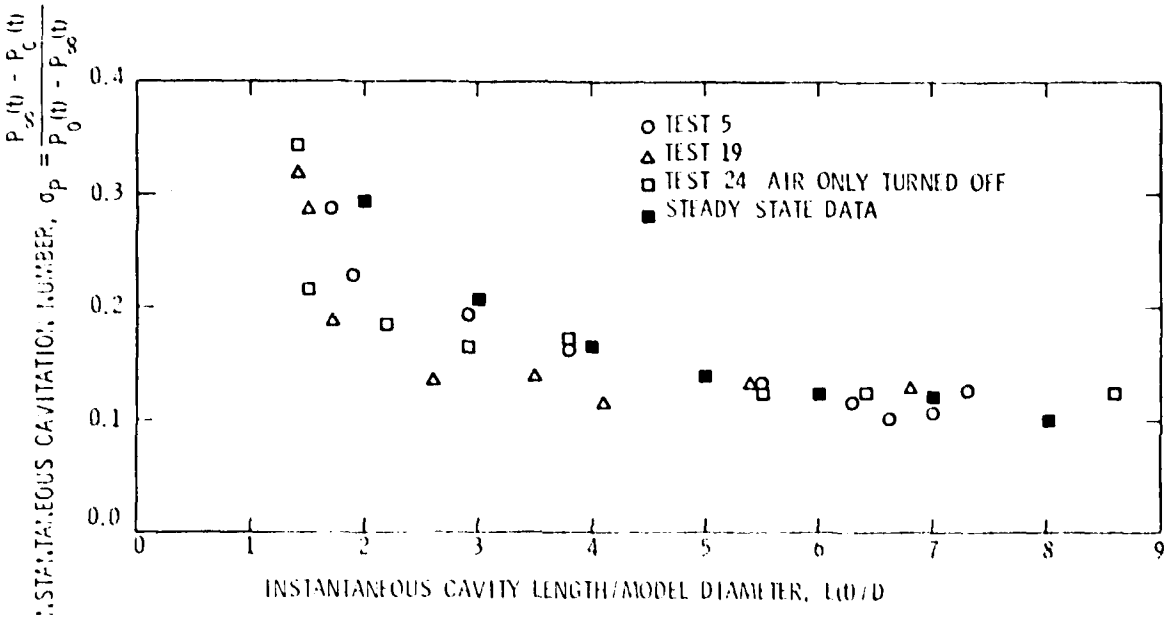

Figure 26 - Instantaneous Cavitation Number, σ_p, Versus Instantaneous Cavity Length for 1.0 inch Diameter 45° Conical Head Model with No Afterbody (Model III), $V_\infty(0)$ = 50 ft/sec

December 3, 1979
DRS:JWH:cac

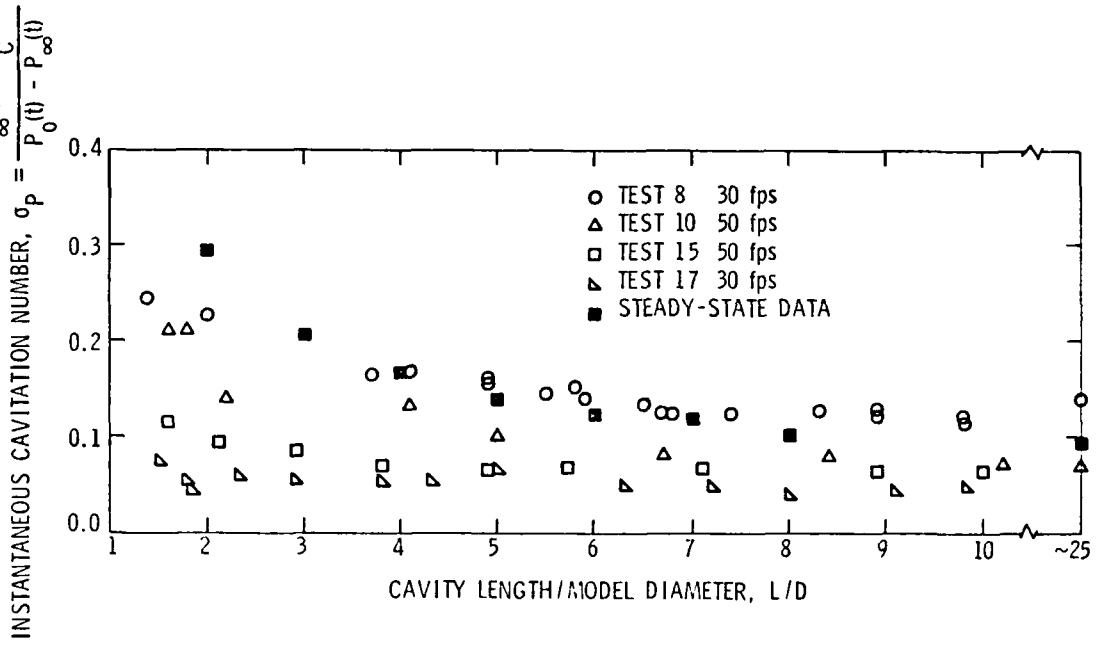

Figure 27 - Instantaneous Cavitation Number, σ_p, Versus Instantaneous Cavity Length for 1.0 inch Diameter, 45° Conical Head Models with No Afterbody (Model III) - Cavity Initially in Twin Vortex Regime

DISTRIBUTION LIST FOR UNCLASSIFIED TM 79-206 by D. R. Stinebring and J. W. Holl, dated December 3, 1979

Commander
Naval Sea Systems Command
Department of the Navy
Washington, DC 20362
Attn: Library
Code NSEA-09G32
(Copy Nos. 1 and 2)

Naval Sea Systems Command
Attn: A. R. Paladino
Code NSEA-05H1
(Copy No. 3)

Naval Sea Systems Command
Attn: T. E. Peirce
Code NSEA-63R3
(Copy No. 4)

Commanding Officer
Naval Underwater Systems Center
Newport, RI 02840
Attn: Library
Code 54
(Copy No. 5)

Commanding Officer and Director
David W. Taylor Naval Ship R&D Center
Department of the Navy
Bethesda, MD 20084
Attn: Library
Code 522
(Copy No. 6)

Commanding Officer
Naval Ocean Systems Center
San Diego, CA 92152
Attn: Library
(Copy No. 7)

Defense Technical Information Center
5010 Duke Street
Cameron Station
Alexandria, VA 22314
(Copy Nos. 8 through 19)

Commander
Naval Surface Weapons Center
White Oak
Silver Spring, MD 20910
Attn: Library
(Copy No. 20)

Naval Surface Weapons Center
Attn: V. C. D. Dawson
Code U-1
(Copy No. 21)

Naval Surface Weapons Center
Attn: J. E. Goeller
Code WA-42
(Copy No. 22)

Naval Surface Weapons Center
Attn: J. Baldwin
Code WA-42
(Copy No. 23)

Naval Surface Weapons Center
Attn: J. A. Iandola
Code WA-42
(Copy No. 24)

Naval Surface Weapons Center
Attn: H. K. Steves
Code WA-42
(Copy No. 25)

Naval Surface Weapons Center
Attn: C. W. Smith
Code WA-42
(Copy No. 26)

Applied Research Laboratory
The Pennsylvania State University
Post Office Box 30
State College, PA 16801
Attn: J. W. Holl
(Copy Nos. 27 through 32)

Applied Research Laboratory
Attn: M. L. Billet
(Copy No. 33)

Applied Research Laboratory
Attn: W. R. Hall
(Copy No. 34)

Applied Research Laboratory
Attn: D. R. Stinebring
(Copy No. 35)

Applied Research Laboratory
Attn: R. E. Henderson
(Copy No. 36)

DISTRIBUTION LIST FOR UNCLASSIFIED TM 79-206 by D. R. Stinebring and J. W. Holl, dated December 3, 1979

Applied Research Laboratory
Attn: F. E. Smith
(Copy No. 37)

Applied Research Laboratory
Attn: C. B. Yungkurth
(Copy No. 38)

Applied Research Laboratory
Attn: A. L. Treaster
(Copy No. 39)

Applied Research Laboratory
Attn: B. R. Parkin
(Copy No. 40)

Applied Research Laboratory
Attn: Garfield Thomas Water Tunnel Files
(Copy No. 41)